a Ca^{2+}- and Mg^{2+}-free solution containing 0.01% EDTA. The detached cells were diluted in the culture medium, and then reseeded with a cell density of approximately 2500 cells/cm^2 on coverslips (9 × 9 mm) coated with fibronectin (Biomedical technologies, Stoughton, MA, USA). The cells were maintained in culture for 1–4 days before use.

2.3. Intracellular Ca^{2+} determination by fluorescence photometry

To determine intracellular Ca^{2+} levels, cultured smooth muscle cells were loaded with 10 μM fura-2 acetoxymethyl ester at 37 °C for 30 min in HEPES-buffered saline (HBS). HBS containing 5 mM $CaCl_2$ instead of 1 mM $CaCl_2$ was used as a standard bath solution. Thereafter, cells were rinsed several times with HBS to remove extracellular fura-2 and used for experiments within 3 h. Changes of intracellular free calcium concentration $[Ca^{2+}]_i$ in individual cells were measured using an Aquacosmos System (Hamamatsu Photonics kk, Shizuoka, Japan) equipped with a Nikon epifluorescence microscope (TE2000-U; Nikon, Tokyo, Japan) and band-pass filters for wavelengths of 340 and 380 nm. After correction for the individual background fluorescence, the ratio of the fluorescence at both excitation wavelengths (F_{340}/F_{380}) was monitored simultaneously to determine the $[Ca^{2+}]_i$. In the present experiments, the amplitude of $[Ca^{2+}]_i$ induced by the first application of 1 μM histamine was defined as 100%. Values were expressed as percents of $[Ca^{2+}]_i$ in the first application.

2.4. Radioligand binding assays to human recombinant receptors

Cloned human recombinant histamine receptors were commercially obtained (H_1: Cat. No. ES-390-M; H_2: Cat. No. ES-391-M, Euroscreen SA, Gosselies, Belgium). Radioligand binding studies to H_1 and H_2 receptors were carried out with [^{3}H]pyrilamine (Cat. No. TRK608; GE Healthcare Bio-Sciences) and [^{3}H]tiotidine (Cat. No. NET688; PerkinElmer Life & Analytical Sciences), respectively. Detailed methods for radioligand binding assays have been described by Nguyen et al. (2001) with minor modifications. Affinity of the competing ligand was expressed as the percent inhibition of radioligand binding, $[(B - N)/(B_0 - N)] \times 100$, where B is the total bound radioactivity in the presence of competing ligand, B_0 is the mean total bound radioactivity in the absence of competing ligand, and N is the mean non-specifically bound radioactivity.

2.5. Drugs

The following drugs and chemicals were used: carbachol hydrochloride, histamine, ethylene glycol-bis (2-aminoethylether)-*N,N,N,N*-tetraacetic acid (EGTA), endothelin-1, cimetidine, pyrilamine (all from Sigma Chemical Co., St. Louis, USA), phenylephrine hydrochloride, N^G-nitro-L-arginine methylester (L-NAME), diltiazem (all from Wako Chemical, Osaka, Japan), and levobunolol hydrochloride (Kaken Pharm, Tokyo, Japan). Concentrations were expressed as final molar concentrations in the organ chambers.

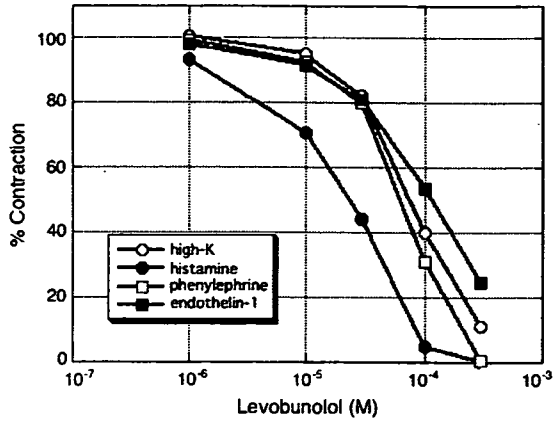

Fig. 1. Levobunolol-induced relaxation of pre-contracted rabbit ciliary arteries. Levobunolol induced concentration-dependent relaxation in the arterial rings that were pre-contracted with high-K solution ($n = 8$), 1 μM histamine ($n = 8$), 10 μM phenylephrine ($n = 11$) or 100 nM endothelin-1 ($n = 10$). The amplitude of contraction induced by High-K solution was defined as 100%.

2.6. Statistical analysis

Results were expressed as means ± S.D. with n representing the number of vessels or cells studied. The concentrations of drugs causing 50% of the maximum relaxation (EC_{50}) were expressed as the log M concentration. Statistical differences between values were determined by the unpaired two-tailed Student's t-test. Differences between the concentration–response curves were analyzed by two-way analysis of variance (ANOVA). $P < 0.05$ was considered statistically significant.

3. Results

Stimulation with 1 μM histamine, 10 μM phenylephrine or 100 nM endothelin-1 elicited nearly the same level of contraction in this preparation as that induced by the high-K solution. Levobunolol caused a concentration-dependent relaxation of the vascular rings that were pre-contracted by each of these agents (Fig. 1). The minimum concentration of levobunolol that induced relaxation was 10 μM. Contractions induced by histamine, phenylephrine, high-K solution, and endothelin-1 were relaxed by 99.7%, 99.6%, 88.9% and 75.1%, respectively

Table 1
Inhibitory effect of levobunolol on radioligand binding to histamine receptors

Receptor (^{3}H-ligand)	Inhibition (%)	
	Levobunolol	Receptor-specific ligand
Histamine H_1 ([^{3}H]pyrilamine)	0.0	99.8 (pyrilamine)
Histamine H_2 ([^{3}H]tiotidine)	28.8	99.2 (cimetidine)

Competing ligand concentration: 10 μM.

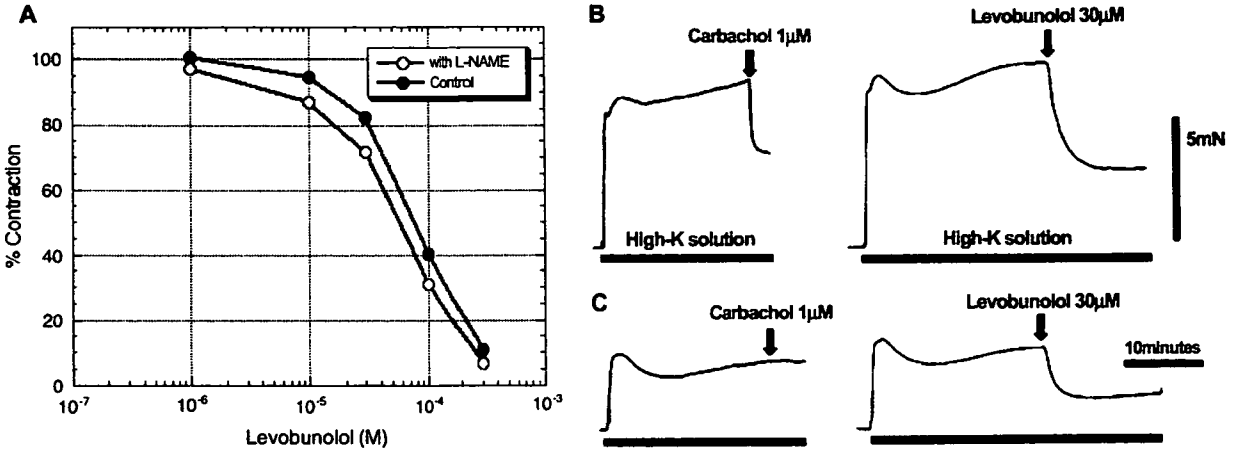

Fig. 2. Effects of L-NAME or denudation of endothelium on levobunolol-induced relaxation of rabbit ciliary arteries. (A) L-NAME (300 μM; $n = 6$) did not significantly alter ($P > 0.05$) the concentration-response curve for relaxation of high-K contracted ciliary arteries. The amplitude of contraction induced by high-K solution was defined as 100%. (B) Both carbachol (1 μM) and levobunolol (30 μM) induced relaxation in high-K pre-contracted ciliary artery. (C) In ciliary arteries denuded of the endothelium, carbachol (1 μM) did not induce relaxation. Denudation did not affect the response to levobunolol. The vertical bar with 5mN represents the actual isometric tension of rabbit ciliary arteries in myograph system.

with 30 mM levobunolol. Levobunolol was more effective in relaxing histamine-induced contractions ($EC_{50} = 20.7 \pm 16.3$ μM, $n = 8$) compared to phenylephrine, high-K or endothelin-1 induced contractions ($EC_{50} = 60.8 \pm 15.3$ μM, $n = 11$; $EC_{50} = 80.3 \pm 12.6$ μM, $n = 8$; $EC_{50} = 106.7 \pm 23.2$ μM, $n = 10$, respectively; Fig. 1).

Cimetidine (100 μM), a histamine H_2 receptor antagonist, did not relax the ciliary arteries pre-contracted with histamine (data not shown). On the other hand, 10 nM pyrilamine, a histamine H_1 antagonist, completely relaxed the histamine-contracted ciliary arteries (data not shown). These results indicated that the H_1 receptor was responsible for histamine induced vascular contraction. To determine if the relaxation effect of levobunolol could be mediated through either of the histamine receptors, we measured the displacement of receptor-specific radiolabeled ligands by levobunolol. Levobunolol had no effect on [^{3}H]pyrilamine binding to the histamine H_1 receptor (Table 1), but it did inhibit 28.8% of ^{3}H-tiotidine binding to the histamine H_2 receptor.

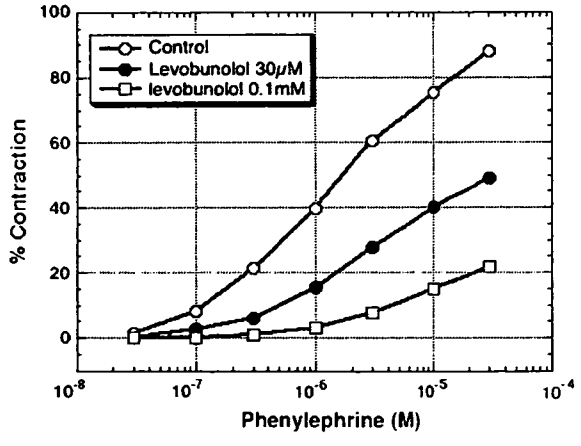

Fig. 3. Effects of levobunolol on phenylephrine concentration-dependent contractions of rabbit ciliary arteries. Levobunolol at 30 μM ($n = 10$) and at 100 μM ($n = 10$) significantly reduced the contractile response to phenylephrine ($P < 0.05$, $n = 14$). The amplitude of contraction induced by high-K solution was defined as 100%.

Pretreatment with 300 μM L-NAME did not changed the levobunolol induced concentration-dependent relaxation of the ciliary artery (Fig. 2A). Denudation of the vascular endothelium also had no effect on the 30 μM levobunolol-induced relaxation although it completely abolished the carbachol-induced relaxation (Fig. 2B,C).

Phenylephrine provoked concentration-dependent contractions in this preparation (Fig. 3). Pretreatment of levobunolol depressed the contractions. However, it did not shift the phenylephrine concentration-response curve to the right.

We compared the relaxing effect of 0.1 mM levobunolol and 1 μM diltiazem in the same preparations that were pre-contracted with either high-K solution or 1 μM histamine (Fig. 4). These concentrations were chosen because they produced approximately 50% relaxation in the high-K pre-contracted arterial rings. Levobunolol induced 59.2 ± 3.6% relaxation of the high-K pre-contracted preparations ($n = 6$), and 89.7 ± 4.2% of the 1 μM histamine ($n = 6$) pre-contracted preparations (Fig. 4A,B). In contrast, diltiazem induced 63.4 ± 7.6% relaxation of the high-K pre-contracted preparations ($n = 6$), but only 40.0 ± 7.2% of the 1 μM histamine ($n = 6$) pre-contracted preparations (Fig. 4C,D).

In Ca^{2+}-free solutions, 1 μM histamine induced a transient contraction of the ciliary artery (Fig. 5). Pretreatment of levobunolol (0.1 mM) markedly inhibited this contraction by 74.6 ± 11.0% (Fig. 5A,B). After a 30 min washout of the levobunolol, the transient contractions were almost completely restored.

In Ca^{2+}-containing Krebs solution, $[Ca^{2+}]_i$ of cultured human aortic smooth muscle cells was elevated by 1 μM

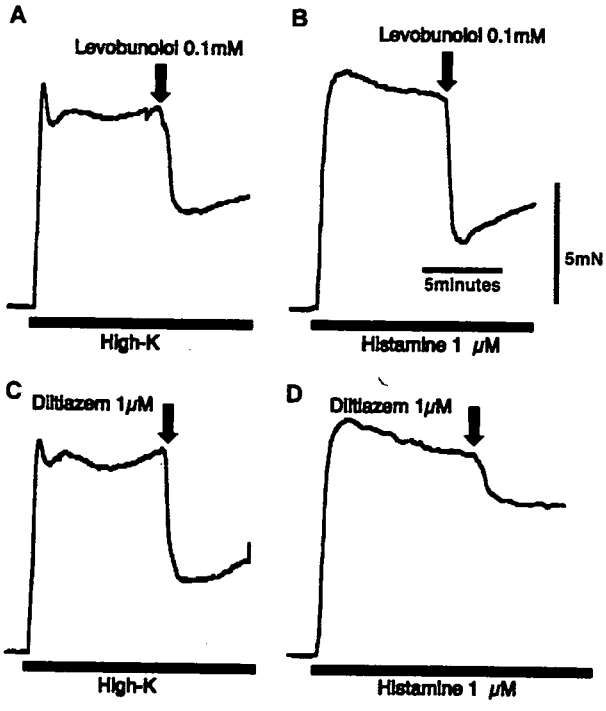

Fig. 4. Effects of levobunolol and diltiazem on high-K or histamine pre-contracted rabbit ciliary arteries. (A) Levobunolol (0.1 mM) induced less relaxation in preparations pre-contracted with high-K ($n = 6$) than with (B) histamine (1 μM, $n = 6$). (C) On the other hand, diltiazem (1 μM) induced a greater relaxation in high-K contracted arteries ($n = 6$) compared to (D) histamine (1 μM) contracted arteries ($n = 6$). The vertical bar with 5mN represents the actual isometric tension of rabbit ciliary arteries in myograph system.

histamine. After a 7 min washout, the amplitude of the $[Ca^{2+}]_i$ response to a second application of 1 μM histamine decreased by 27.6 ± 6.9% (Fig. 6A). To determine the effect of levobunolol on the histamine induced $[Ca^{2+}]_i$ increase, 3 μM levobunolol was added to the incubation medium just after washing out the first application of histamine. The amplitude of the $[Ca^{2+}]_i$ due to the second application of histamine in the presence of 3 μM levobunolol was decreased 45.9 ± 18.9%, a significantly greater decrease than the control (Fig. 6B, Table 2); whereas in Ca^{2+}-free solution, 3 μM levobunolol had no effect on $[Ca^{2+}]_i$ increase with 1 μM histamine (Fig. 6C,D, Table 2). Pyrilamine (10 nM) completely inhibited the elevation of $[Ca^{2+}]_i$ by 1 μM histamine in both the Ca^{2+}-containing Krebs solution and in the Ca^{2+}-free solution (Fig. 6E,F).

4. Discussion

The present studies demonstrated that levobunolol, a β-adrenergic antagonist, relaxed rabbit ciliary arteries that were pre-contracted with high-K solution, histamine, phenylephrine, or endothelin-1. These agents contract vascular smooth muscle by variety of mechanisms. The high-K solution induces contractions that depend on the passage of extracellular Ca^{2+} through voltage-dependent Ca^{2+} channels (Gustafsson, 1993). Histamine provokes contractions using Ca^{2+} that enters through voltage-dependent and receptor-dependent Ca^{2+} channels, as well as from intracellular Ca^{2+} stores (Laporte and Laher, 1997). Phenylephrine induces contraction through activation of α_1-adrenergic receptors that open voltage-dependent Ca^{2+} channels and induce Ca^{2+} release from intracellular Ca^{2+} stores (Eckert et al., 2000). Endothelin-1 is one of the most potent vasoconstrictors (Highsmith et al., 1989; Murakawa et al., 1990). When it binds to either G-protein-linked endothelin

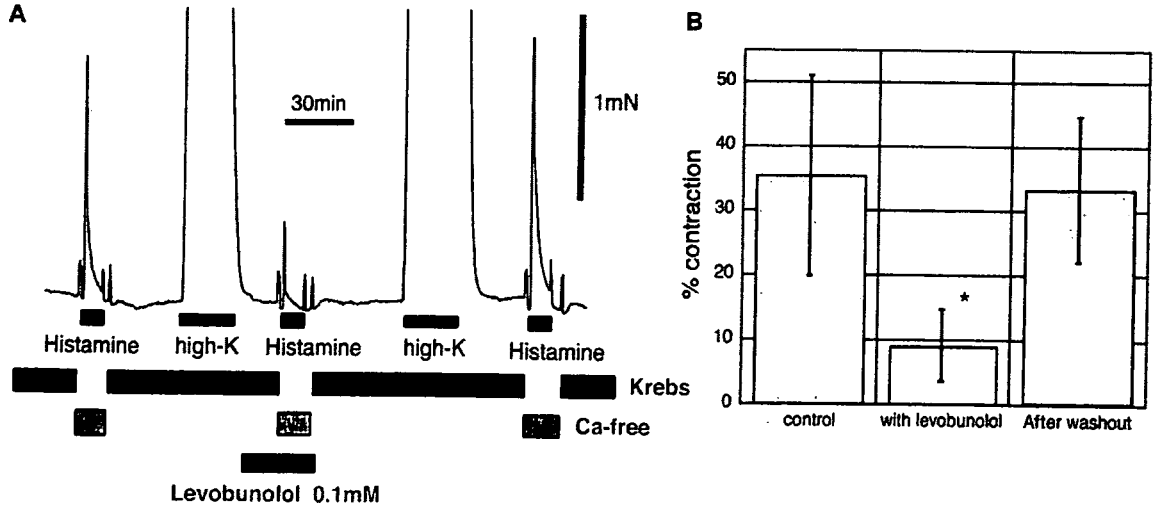

Fig. 5. Effects of levobunolol on histamine-induced transient contraction of rabbit ciliary arteries in Ca^{2+}-free solution. (A) Histamine (1 μM) was applied 6 min after incubation in Ca^{2+}-free solution. This was followed by high-K solution-induced contraction. Afterwards, the preparation was washed out with Krebs solution containing levobunolol (0.1 mM). (B) The amplitude of histamine-induced contraction in Ca^{2+}-free solution was then compared to the contractions in the presence or absence of levobunolol. Levobunolol significantly reduced the histamine-induced contraction in Ca^{2+}-free medium ($^*P < 0.05$, $n = 22$). The amplitude of contraction induced by high-K solution was defined as 100%. The vertical bar with 1mN represents the actual isometric tension of rabbit ciliary arteries in myograph system.

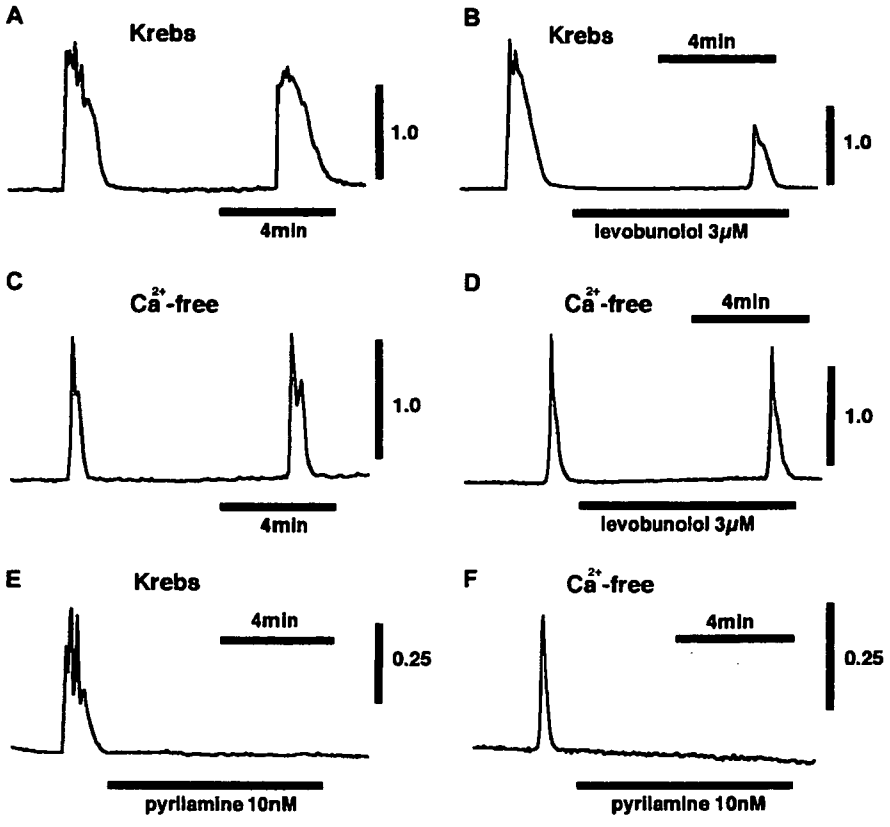

Fig. 6. Effects of levobunolol and pyrilamine on the histamine-induced increase of $[Ca^{2+}]_i$ in human aortic smooth muscle cells. Histamine (1 μM) was applied twice with a 7 min interval between application. Levobunolol (3 μM) or pyrilamine (10 nM) were pre-incubated before the second application of histamine. (A, B) In Krebs medium, levobunolol reduced the $[Ca^{2+}]_i$ in response to histamine. (C, D) In Ca^{2+}-free medium, levobunolol did not reduced the $[Ca^{2+}]_i$ in response to histamine. (E, F) Pyrilamine (10 nM) reduced the $[Ca^{2+}]_i$ in response to histamine in both Krebs medium and in Ca^{2+}-free medium. The vertical bar with either 1.0 or 0.25 represents the ratio of F_{340}/F_{380} which was monitored to determine the $[Ca^{2+}]_i$ in Aquacosmos System.

A or endothelin B receptors, it induces smooth muscle contraction by releasing Ca^{2+} from intracellular stores and promoting entry from the extracellular medium (Masaki, 2004).

Levobunolol was more effective on histamine-induced contractions compared to others. However, its relaxation effect is unlikely to be mediated through the H_1 receptor because levobunolol does not displace [^{3}H]pyrilamine binding to that receptor. In the absence of any affinity for the H_1 receptor, levobunolol must antagonize the histamine-induced contraction through some other mechanism.

NO is formed from L-arginine by NO synthase in vascular endothelial cells and mediates the endothelium-dependent relaxation of vascular smooth muscle (Palmer et al., 1988). L-NAME, a NO synthase inhibitor, had no effect on the levobunolol-induced relaxation. Further, to investigate whether any endothelium-derived factor was involved in the relaxation mechanism, we denuded the vascular endothelium. This also had no effect on levobunolol-induced relaxation. These results suggested that NO or other endothelium-derived factors are not involved in the levobunolol relaxing mechanism.

In the present studies, phenylephrine, an α_1-adrenergic agonist, induced concentration-dependent contractions in rabbit ciliary artery. Levobunolol may have some α_1-antagonistic action in addition to the well known β-antagonistic action (Mitsuoka et al., 1997). However, levobunolol only depressed the phenylephrine concentration–response curve and did not shift this curve to the right. Therefore, it seems that the α_1-adrenergic receptor does not participate in the relaxant effect of levobunolol.

It has been reported that levobunolol inhibits the intracellular Ca^{2+} increases by blocking the L-type voltage-dependent Ca^{2+} channel (Wu et al., 2004). In present studies, we found that levobunolol was more effective in relaxing the histamine-induced contraction compared to the high-K-induced contraction. On the other hand, diltiazem, a typical L-type voltage-dependent Ca^{2+} channel blocker (Gunthorpe and Lummis, 1999), had a greater effect on the high-K-induced contraction. Diltiazem blocks L-type voltage-dependent Ca^{2+} channels, but these channels were not blocked by levobunolol in our cultured human aortic smooth muscle cells, though at higher concentrations they may do so. These differences between levobunolol and diltiazem suggest that the relaxing mechanism of levobunolol is different from that of diltiazem.

Our fluorescence photometry studies using cultured human aortic smooth muscle cells indicated that levobunolol

Table 2
Inhibitory effects of levobunolol or pyrilamine on histamine-induced increase of $[Ca^{2+}]_i$

Incubation medium	Control	3 μM Levobunolol	10 nM Pyrilamine
Krebs solution	72.5 ± 6.9 (35)	45.9 ± 18.9* (41)	20.8 ± 30.3* (27)
Ca^{2+}-free solution	83.5 ± 9.2 (34)	99.8 ± 37.0 (35)	15.3 ± 23.8* (28)

The amplitude of $[Ca^{2+}]_i$ induced by the first application of 1 μM histamine was defined as 100%. Values were expressed as per cents of $[Ca^{2+}]_i$ in the first application. *$P < 0.05$ compared to control.

decreased the $[Ca^{2+}]_i$ that was elevated by histamine in Ca^{2+}-containing Krebs solution, but it had no effect in Ca^{2+}-free solution. Thus, we conclude that the relaxation mechanism of levobunolol is partly due to the blocking of extracellular Ca^{2+} entry through non-voltage-dependent Ca^{2+} channels. These data also suggest that levobunolol does not inhibit Ca^{2+} release from intracellular stores. However, levobunolol did inhibit the rabbit ciliary artery contraction induced by histamine in Ca^{2+}-free solution. These apparent discrepancies may be due to species-specific differences in smooth muscle physiology. They may also be due to differences in the responsiveness of cultured cells compared to in situ cells.

Pyrilamine, a histamine H_1 antagonist, relaxed histamine pre-contracted preparations, and it also strongly inhibited the histamine-induced increase of $[Ca^{2+}]_i$ in the cultured human aortic smooth muscle cells in both Ca^{2+}-containing Krebs and in Ca^{2+}-free solution. This suggests that levobunolol, which did not affect $[Ca^{2+}]_i$ in Ca^{2+}-free media, induces relaxation by changing Ca^{2+} sensitivity or by other intracellular Ca^{2+} independent mechanisms.

In summary, the vasodilatory mechanism of levobunolol was independent of NO or vascular endothelium, and it was not dependent on α_1-adrenergic receptor antagonism. Moreover, levobunolol did not have histamine receptor antagonistic action. We conclude that levobunolol relaxes rabbit ciliary artery by two different mechanisms. First, the relaxation may be due to the blockade of Ca^{2+} entry through non-voltage-dependent Ca^{2+} channels. Second, levobunolol may induce relaxation by intracellular Ca^{2+}-independent mechanisms. These actions of levobunolol may explain the mechanisms of increased ocular blood flow in vivo.

Acknowledgments

The authors thank Kaken Pharm Co. for providing levobunolol for these experiments, and Ms. Sanae Takaseki for her excellent technical assistance. Supported by Japan Society for the Promotion of Science Grant-in-Aid for Scientific Research #12671718 and 12671719.

References

Arend, O., Harris, A., Arend, S., Remky, A., Martin, B.J., 1998. The acute effect of topical beta-adrenoreceptor blocking agents on retinal and optic nerve head circulation. Acta Ophthalmol. Scand. 76, 43–49.

Bosem, M.E., Lusky, M., Weinreb, R.N., 1992. Short-term effects of levobunolol on ocular pulsatile flow. Am. J. Ophthalmol. 114, 280–286.

Chiou, G.C., Zhao, F., Shen, Z.F., Li, B.H., 1990. Effects of D-timolol and L-timolol on ocular blood flow and intraocular pressure. J. Ocul. Pharmacol. 6 (1), 23–30.

Collignon-Brach, J., 1994. Longterm effect of topical beta-blockers on intraocular pressure and visual field sensitivity in ocular hypertension and chronic open-angle glaucoma. Surv. Ophthalmol. 38, S149–S155.

Drance, S.M., 1998. A comparison of the effects of betaxolol, timolol, and pilocarpine on visual function in patients with open-angle glaucoma. J. Glaucoma. 7, 247–252.

Eckert, R.E., Karsten, A.J., Utz, J., Ziegler, M., 2000. Regulation of renal artery smooth muscle tone by α_1-adrenoceptors: role of voltage-gated calcium channels and intracellular calcium stores. Urol. Res. 28, 122–127.

Flammer, J., 1994. The vascular concept of glaucoma. Surv. Ophthalmol. 38, S3–S6.

Georgopoulos, G.T., Diestelhorst, M., Fisher, R., Ruokonen, P., Krieglstein, G.K., 2002. The short-term effect of latanoprost on intraocular pressure and pulsatile ocular blood flow. Acta Ophthalmol. Scand. 80, 54–58.

Grunwald, J.E., 1990. Effect of timolol maleate on the retinal circulation of human eyes with ocular hypertension. Invest. Ophthalmol. Vis. Sci. 31, 521–526.

Gunthorpe, M.J., Lummis, S.C., 1999. Diltiazem causes open channel block of recombinant 5-HT3 receptors. J. Physiol. 519, 713–722.

Gustafsson, H., 1993. Vasomotion and underlying mechanisms in small arteries. An in vitro study of rat blood vessels. Acta Physiol. Scand. Suppl. 614, 1–44.

Hayashi-Morimoto, R., Yoshitomi, T., Ishikawa, H., Hayashi, E., Sato, Y., 1999. Effects of beta antagonists on mechanical properties in rabbit ciliary artery. Graefes Arch. Clin. Exp. Ophthalmol. 237, 661–667.

Highsmith, R.F., Pang, D.C., Rapoport, R.M., 1989. Endothelial cell-derived vasoconstrictors: Mechanisms of action in vascular smooth muscle. J. Cardiovasc. Pharmacol. 13 (Suppl 5), S36–S44.

Ishikawa, H., Yoshitomi, T., Mashimo, K., Nakanishi, M., Shimizu, K., 2002. Pharmacological effects of latanoprost, prostaglandin E2, and F2α on isolated rabbit ciliary artery. Graefes Arch. Clin. Exp. Ophthalmol. 240, 120–125.

Keef, K.D., Bowen, S.M., 1989. Effect of ACh on electrical and mechanical activity in guinea pig coronary arteries. Am. J. Physiol. 257, H1096–H1103.

Kimura, I., Shinoda, K., Tanino, T., Ohtake, Y., Mashima, Y., 2005. Effect of topical unoprostone isopropyl on optic nerve head circulation in controls and in normal-tension glaucoma patients. Jpn. J. Ophthalmol. 49, 287–293.

Laporte, R., Laher, I., 1997. Sarcoplasmic reticulum-sarcolemma interactions and vascular smooth muscle tone. J. Vasc. Res. 34, 325–343.

Masaki, T., 2004. Historical review: Endothelin. Trends Pharmacol. Sci. 25, 219–224.

Mitsuoka, Y., Matsuzawa, S., Tachiiri, T., Momo, K., 1997. Effects of AG-901 ophthalmic solution on intraocular pressure in ocular hypertensive rabbits and ocular blood flow in ocular normotensive rabbits. Atarashii Ganka 14, 801–806.

Morsman, C.D., Bosem, M.E., Lusky, M., Weinreb, R.N., 1995. The effect of topical beta-adrenoceptor blocking agents on pulsatile ocular blood flow. Eye 9, 344–347.

Mulvany, M.J., Halpern, W., 1976. Mechanical properties of vascular smooth muscle cells in situ. Nature 260, 617–619.

Mulvany, M.J., Halpern, W., 1977. Contractile properties of small arterial resistance vessels in spontaneously hypertensive and normotensive rats. Circ. Res. 41, 19–26.

Murakawa, K., Kohno, M., Yokokawa, K., Yasunari, K., Horio, T., Kurihara, N., Takeda, T., 1990. Endothelin-induced renal vasoconstriction and increase in cytosolic calcium in renal vascular smooth muscle cell. Clin. Exp. Hypertens. A. 12, 1037–1048.

Nguyen, T., Shapiro, D.A., George, S.R., Setola, V., Lee, D.K., Cheng, R., Rauser, L., Lee, S.P., Lynch, K.R., Roth, B.L., Odowd, B.F., 2001. Discovery of a novel member of the histamine receptor family. Mol. Pharmacol. 59, 427–433.

Ogasawara, H., Yoshida, A., Fujio, N., Konno, S., Ishiko, S., 1999. Effect of topical levobunolol on retinal, optic nerve head, and choroidal circulation in normal volunteers. Nippon Ganka Gakkai Zasshi 103, 544–550.

Palmer, R.M., Rees, D.D., Ashton, D.S., Moncada, S., 1988. L-Arginine is the physiological precursor for the formation of nitric oxide in endothelium-dependent relaxation. Biochem. Biophys. Res. Commun. 153, 1251–1256.

Sato, T., Muto, T., Ishibashi, Y., Roy, S., 2001. Short-term effect of beta-adrenoreceptor blocking agents on ocular blood flow. Curr. Eye Res. 23 (4), 298–306.

Setoguchi, M., Ohya, Y., Abe, I., Fujishima, M., 1995. Inhibitory action of betaxolol, a beta 1-selective adrenoceptor antagonist, on voltage-dependent calcium channels in guinea-pig artery and vein. Br. J. Pharmacol. 115 (1), 198–202.

Shaikh, M.H., Mars, J.S., 2001. The acute effect of pilocarpine on pulsatile ocular blood flow in ocular hypertension. Eye 15, 63–66.

Wu, K.Y., Wang, H.Z., Hong, S.J., 2004. Inhibition of endothelin-1 and KCl-induced increase of $[Ca^{2+}]_i$ by antiglaucoma drugs in cultured A7r5 vascular smooth-muscle cells. J. Ocul. Pharmacol. Ther. 20, 201–209.

Yoshitomi, T., Ishikawa, H., Hayashi, E., 2000. Pharmacological effects of pilocarpine on rabbit ciliary artery. Curr. Eye Res. 20, 254–259.

Yoshitomi, T., Yamaji, K., Ishikawa, H., Ohnishi, Y., 2002. Vasodilatory effects of nipradilol, an alpha- and beta-adrenergic blocker with nitric oxide releasing action, in rabbit ciliary artery. Exp. Eye Res. 75, 669–676.

Yoshitomi, T., Yamaji, K., Ishikawa, H., Ohnishi, Y., 2004. Vasodilatory mechanism of unoprostone isopropyl on isolated rabbit ciliary artery. Curr. Eye Res. 28, 167–174.

Available online at www.sciencedirect.com
ScienceDirect
Experimental Eye Research 84 (2007) 626–634
EXPERIMENTAL EYE RESEARCH
www.elsevier.com/locate/yexer

Existence of small slow-cycling Langerhans cells in the limbal basal epithelium that express ABCG2

Wensheng Chen [a,b], Koji Hara [b], Qing Tian [c], Kanxing Zhao [a,*], Takeshi Yoshitomi [b]

[a] Tianjin Medical University, Tianjin Eye Hospital, Tianjin, China
[b] Department of Ophthalmology, Akita University School of Medicine, Hondo 1-1-1, Akita 010, Japan
[c] Nanyang Eye Hospital, City of Nanyang, Henan Province, China

Received 26 July 2006; accepted in revised form 13 November 2006
Available online 23 January 2007

Abstract

Despite the obvious importance of limbal stem cells in corneal homeostasis and tumorigenesis, little is known about their specific biological characteristics. The purpose of this study was to characterize limbal slow-cycling cells based on the expression of ABCG2 and major histocompatibility complex (MHC) class II and the cell size. Wistar rats were daily injected with 5-bromo-2-deoxyuridine (BrdU) at a dose of 5 mg/100 g for 2 weeks. After 4-week BrdU-free period, corneal tissues were excised, and immunofluorescence staining for ABCG2, BrdU, and MHC class II was performed by confocal microscopy. In another series, corneal tissues of normal rat were double immunostained for ABCG2, keratin 14, keratin 3, CD11c, and MHC class II. In addition, limbal, peripheral and central corneal epithelial sheets were isolated by Dispase II digestion and dissociated into single cell by trypsin digestion and cytospin preparations were double immunostained for ABCG2 and MHC class II. The cell size and nucleus-to-cytoplasm (N/C) ratio of limbal ABCG2$^+$ cells were analyzed and compared with those of cells from other zones. BrdU label-retaining cells (LRCs) with expression of ABCG2 were found in the limbal epithelial basal layer, but not in other parts of the cornea. Approximately 20% of these cells were MHC class II positive. All MHC class II$^+$ cells in the corneal epithelium were positive for CD11c, a marker for dendritic cells (DCs). Double labeling with ABCG2 and keratin 14 showed that nearly four-fifth of limbal ABCG2$^+$ cells were positive for keratin 14 but negative for keratin 3, exhibiting an undifferentiated epithelial cell lineage. Cytospin sample analysis revealed the presence of a distinct population of smaller ABCG2$^+$ cells with expression of MHC class II with a larger N/C ratio in the limbal epithelium. A new population of small slow-cycling cells with large N/C ratio has been found to express ABCG2 in the limbal epithelial basal layer. Some of these cells normally express MHC class II antigen. These findings may have important implications for our understanding of the characteristics of limbal slow-cycling cells.

Keywords: limbal stem cell; slow-cycling cells; ABCG2; major histocompatibility complex class II; CD11c; Langerhans cell

1. Introduction

It is easy to be fascinated by limbal stem cells, not only because they play a pivotal role in corneal epithelial homeostasis and tumorigenesis, but also because they are exclusively concentrated in the limbal epithelial basal layer and are completely separated from their progeny cells, transient amplifying (TA) cells in the peripheral and central corneal epithelia. Such a compartmentalization of limbal stem cells provides an excellent model for studying the growth and differentiation of stem cells and TA cells. As yet, corneal epithelial stem cells have been detected in the limbal epithelial basal layer by determination of slow-cycling cells (label-retaining cells [LRCs]) by mitotic DNA labeling (Cotsarelis et al., 1989; Lavker et al., 1991; Chen et al., 2003), comparison of proliferative capacity in vivo and in vitro (Ebato et al., 1988; Lavker et al., 1998; Hernandez Galindo et al., 2003), comparison of

* Corresponding author. Present address: Tianjin Eye Hospital, No 4, Gansu Road, Heping District, Tianjin 300020, People's Republic of China. Tel: +86 22 27313336; fax: +86 22 27313133.
E-mail address: ZKX@tijmu.edu.cn (K. Zhao).

0014-4835/$ - see front matter © 2006 Elsevier Ltd. All rights reserved.
doi:10.1016/j.exer.2006.11.006

cell size and nucleus-to-cytoplasm (N/C) ratios (Romano et al., 2003; Arpitha et al., 2005), and expression of some polypeptides (Schlötzer-Schrehardt and Kruse, 2005).

Recently, for the identification of limbal stem cells, a number of investigations have been performed to examine the expression of ABCG2, a member of the ATP binding cassette (ABC) transporters, in the corneal epithelium. Different from most other putative markers for limbal stem cells that label the majority of limbal basal cells, ABCG2 expression is strictly confined to small clusters of basal cells in the limbal epithelium (Chen et al., 2004; Umemoto et al., 2005; de Paiva et al., 2005). Furthermore, limbal $ABCG2^+$ cells grow better than limbal $ABCG2^-$ cells in human cell culture (de Paiva et al., 2005). Therefore, ABCG2 has been considered to be the only maker that is able to distinguish limbal stem cells from TA cells and the most useful cell surface marker for the identification and isolation of limbal stem cells (Schlötzer-Schrehardt and Kruse, 2005).

Although these findings are consistent with the fact that corneal epithelial stem cells are exclusively located in the limbal basal epithelium, no direct evidence is yet available to confirm that limbal $ABCG2^+$ cells are epithelial stem cells, because limbal basal epithelium also contains TA cells, and as well as a small number of Langerhans cells (LCs) and melanocytes (Cotsarelis et al., 1989; Higa et al., 2005). Even more important, the label-retaining property of limbal $ABCG2^+$ cells has never been directly demonstrated.

Under normal condition, limbal stem cells are slow-cycling, that is, cells endowed with a long cell time (which indicates low mitotic activity). Therefore, the identification of these cells can be based on the presence of thymidine or 5-bromo-2-deoxyuridine (BrdU) LRCs (Lehrer et al., 1998; Nagasaki and Zhao, 2005). In the present study, we characterized limbal slow-cycling cells based on the expression of ABCG2 and histocompatibility complex (MHC) class II molecules. We found that all limbal $ABCG2^+$ cells are smaller slow-cycling cells with large N/C ratio. We show that the uninflamed limbal basal epithelium is endowed with a small number of slow-cycling LCs with expression of ABCG2. The significance of the findings is further discussed.

2. Materials and methods

BrdU-labeling reagent was purchased from Zymed Laboratories (South San Francisco, CA, USA); pentobarbital sodium from Abbott Laboratories (North Chicago, IL, USA); Dulbecco modified Eagle medium (DMEM), Dispase II, 0.25% Trypsin-0.02% EDTA, and 5% FBS–HBSS from Invitrogen Corp (Carlsbad, CA); fetal bovine serum (FBS) from HyClone (Logan, UT); biotinylated mouse anti-BrdU antibody (BrdU-labeling kit) from Oncresprod (Boston, MA, USA); FITC-conjugated MHC class II antibody (OX6) from Immunotech (Marseille, France); biotinylated mouse monoclonal anti-rat MHC class II monoclonal antibody (RT1B; OX6) from PharMingen (San Diego, CA); FITC-conjugated anti-ABCG2 antibody (5D3) from MBL (Aichi, Japan); biotinylated mouse monoclonal anti-rat keratin 14 (clone LL002) and keratin 3 from Lab Vision (Fremont, CA); mouse anti-rat CD11c from Cosmobio (Tokyo, Japan); rhodamine-conjugated goat anti-mouse IgG from Biochemical Division (Aurora, Ohio); streptavidin-conjugated Alexa Fluor 594 and streptavidin-conjugated Alexa Fluor 350 from Molecular Probes (Eugene, OR); 4,6-diamidino-2-phenylindole (DAPI) and normal goat serum from Vector Laboratories (Burlingame CA).

2.1. Experimental animals

A total of 30 six-week-old Wistar rats of either sex were used in the study. The animals were housed in individual cages at constant room temperature (19–23 °C) and humidity of 40–50%, and with a constant 12-h light–dark cycle (Animal House, University of Akita, Japan). Before any experimental procedure, the animals were examined for ocular surface disease with handheld biomicroscope and were excluded if any disease was found. All subsequent experiments were conducted in accord with the ARVO statement for the use of Animals in Ophthalmic and Vision Research and received the approval of the Animal Care Facility of Akita University School of Medicine.

2.2. Labeling of slow-cycling cells

To label slow-cycling stem cells, 10 rats received daily injection of BrdU for 2 weeks at a dose of 5 mg/100 g. The animals were left untreated for 4 weeks. Following this chase period, only slow-cycling stem cells retained their label and could be identified by the presence of BrdU LRCs (Lehrer et al., 1998).

2.3. Preparation of cytospin sample

After being killed with an overdose of pentobarbital sodium, corneas were excised from normal rats ($n = 5$). Central cornea was punched out using a 2-mm trephine. Limbal rim was separated from sclera and peripheral cornea using a scalpel under the stereomicroscope. Limbal, peripheral and central corneal tissues were treated with Dispase II (2 mg/mL in DMEM) at 37 °C for 45 min. Epithelial sheet was then removed and treated with 0.25% trypsin/1 mM EDTA solution to harvest dissociated cells. After centrifugation at 780 × g for 10 min, cells were resuspended in DMEM containing 10% FBS to stop enzyme activity. After being washed in PBS, cell suspension was filtered through a 40 μm Cell Strainer (BD Falcon, San Jose, CA) to collect single cell. After centrifugation at 400 × g for 5 min, cells for cytospin preparation (5.0×10^4 cells/slide) were deposited on glass slides using Auto Smear CF-12D (Sakura Finetek, Tokyo, Japan).

2.4. Immunohistochemical studies

After BrdU LRCs containing eyes ($n = 20$) had been enucleated and fixed in PBS with 1% paraformaldehyde for 24 h, under a dissecting microscope (Model SZ40; Olympus, Tokyo, Japan), the retina, lens, and iris were discarded, and four incisions were made in each cornea. Subsequently, the

corneas were washed in PBS with 1% Triton X-100 and 1% dimethyl sulfoxide (DMSO; TD buffer). To block nonspecific staining, corneas were incubated in 1.5% normal goat serum diluted in TD buffer for 1 h. Then, the tissues were incubated with either FITC-conjugated anti-ABCG2 antibody or FITC-conjugated anti-rat MHC class II antibody overnight with agitation (50 turns per minute). The second day, the tissues were washed with distilled water, placed in 0.3 N HCl for 30 min, washed in TD buffer. Next, the tissues were incubated in blocking solution for 1 h. Afterward, the tissues were incubated in biotinylated anti-BrdU antibody for 4 h with agitation. The tissues were then rinsed with TD buffer and placed in streptavidin-conjugated Alexa Fluor 594 for 2 h with agitation. After distilled water wash, the whole-mount cornea tissues were mounted epithelial side up on a slide and stained with a nuclear fluorescence dye, DAPI.

To determine whether limbal ABCG2$^+$ cells express keratin 14 and keratin 3, immunostaining of normal corneal tissues ($n = 30$) for ABCG2, keratin 14, and keratin 3 was performed. Briefly, after being washed in TD buffer, the tissues were incubated in blocking solution for 1 h. Then, a mixture of FITC-conjugated anti-ABCG2 antibody and biotinylated anti-rat keratin 14 (or keratin 3) was applied to the tissues overnight. The next day, they were washed in TD buffer and placed in streptavidin-conjugated Alexa Fluor 350 for 2 h. DAPI was used as a DNA counterstain.

Double staining of normal corneal tissues with CD11c and MHC class II was also performed to determine whether MHC class II$^+$ cells expressed dendritic cell (DC)/LC marker (Camelo et al., 2004). Briefly, corneal tissues were washed in TD buffer and incubated in blocking solution. Then, a mixture of FITC-conjugated anti-rat MHC class II antibody and mouse anti-rat CD11c antibody was applied to the samples overnight. The next day, the tissues were washed in TD buffer and rhodamine-conjugated goat affinity purified anti-mouse IgG was applied to the sample for 2 h, followed counterstaining with DAPI. All incubations were performed at RT. All antibodies were optimally diluted in TD buffer.

All the corneal tissues that had been observed on whole mount were snap-frozen in liquid nitrogen, and 10 μm thick cross-sections were prepared with cryostat. These sections were also examined by confocal microscopy.

Double staining of cytospin preparations separated from normal corneas for MHC class II and ABCG2 were performed to determine the ABCG2$^+$ cells with expression of MHC class II. Briefly, after being washed in PBS, blocking solution was applied to the cytospin preparations for 30 min. The cytospin preparations were then incubated in a mixture of FITC-conjugated anti-ABCG2 antibody and biotinylated anti-rat MHC class II antibody for 1 h. Then, the cytospin preparations were rinsed with PBS and placed in diluted streptavidin-conjugated Alexa Fluor 594. DAPI was used as a DNA counterstain.

2.5. Confocal microscopy

A confocal laser scanning microscopy (LSM510 Axiovert200M; Carl Zeiss Meditec, Göttingen, Germany) was used to image the localization of DAPI (405-nm laser line excitation; 420/80 emission filter), Alexa 488 (488-nm laser line excitation; 505/530 emission filter) and Alexa 594 (594-nm laser line excitation; 560/593 emission filter). Images were captured with identical photomultiplier tube gain setting and processed (LSM-PC; Carl Zeiss Meditec, Inc), using the Z-stack option. Multiple scans from the surface to the basal layer of the corneal epithelium can be obtained by this technique. The rat cornea, which has a diameter of 7 mm, was divided into three different areas. The central cornea was defined as the area within 2 mm of the corneal center. The peripheral cornea was the area between 2 mm of the center and the semi-transparent limbus viewed under transmitted light. The limbus was the area between peripheral cornea and presence of goblet cells in flat whole mounts. Using grid, the number of cells with different markers in surface and basal layers of different epithelial zones was counted. At least five different areas were observed in each sample. Values were expressed as the mean ± SEM of the cells/mm^2. Images were reproduced for publication with image-management software (Photoshop 7.0; Adobe Systems Inc., Mountain View, CA).

Cellular and nuclear areas of single cell in cytospin preparations were measured using the confocal software (LSM Image Browser). Briefly, fluorescence Z-stack (1-μm) images were obtained simultaneously for FITC and Alexa Fluor 594 and DAPI and transmitted light for 50 limbal ABCG2$^+$ cells with expression of MHC class II, limbal ABCG2$^+$ cells without expression of MHC class II, peripheral, and central corneal epithelial cells. The polygon tool from stack was used to draw the region of interest (ROI) around the cell in the transmitted light image and the ROI around the DAPI-stained region for the nuclear area of the same cell.

2.6. Statistical analysis

Fifty cells from the limbal, peripheral and central corneal epithelia were chosen for cell and nuclear areas measurement. N/C ratio was created by dividing the area of nuclear with that of the cell. The Mann–Whitney U test was used to compare mean values. A value of $P < 0.05$ was considered significant.

3. Results

3.1. Distribution of BrdU LRCs in the corneal epithelium

After rats were injected with BrdU daily for 2 weeks, immunohistochemical analysis was performed to determine BrdU-labeled cells in the corneal epithelium. Staining with BrdU antibody revealed that, 14 days after injection of BrdU, over 80% of central corneal epithelial cells, over 75% of peripheral corneal epithelial cells, and over 70% of limbal epithelial cells were BrdU-labeled. After a 4-week BrdU-free period, all of the BrdU-labeled cells disappeared from central and peripheral cornea. However, the limbal basal epithelium was populated with a number of round BrdU-labeled cells (43 ± 10.3cells/mm^2) (Fig. 1).

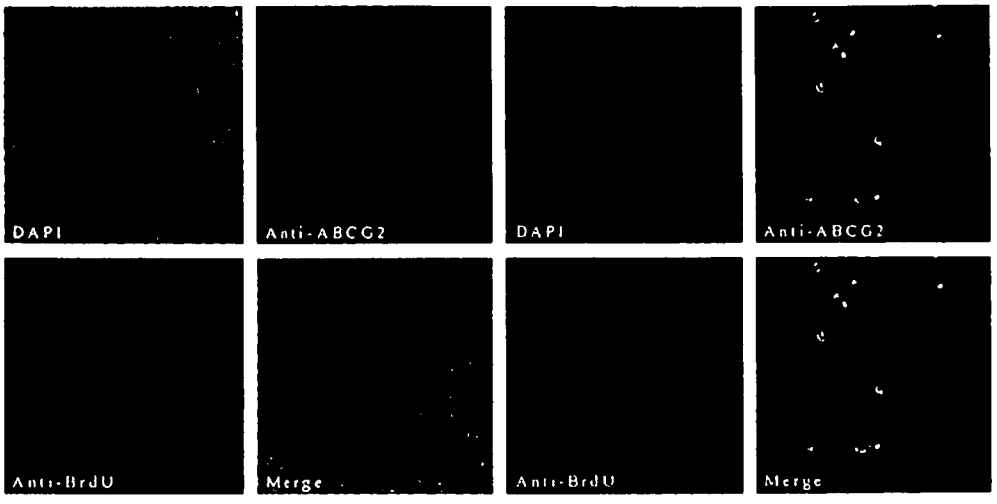

Fig. 1. Distribution of slow-cycling cells in rat corneal epithelium. (left) Peripheral corneal basal epithelium; (right) limbal basal epithelium. After daily injection of BrdU followed by 1-month BrdU-free period, the slow-cycling BrdU-labeled cells are localized in the limbal basal epithelium. Double staining with ABCG2 antibody showed that all BrdU LRCs expressed ABCG2 (pink). In contrast, no such cells can be found in peripheral corneal basal epithelium.

3.2. Expression of ABCG2, MHC class II molecules, CD11c, keratin 14 and keratin 3 in the corneal epithelium

Immunofluorescence labeling of corneal tissues with ABCG2 antibody revealed that ABCG2$^+$ cells were located in the limbal basal epithelium. Double staining of corneal tissues with BrdU antibody showed that the same cells were positive for BrdU label-retaining test. In contrast, there was no expression of ABCG2 in the peripheral and central corneal basal epithelium (Fig. 1). To determine the location of BrdU LRC with expression of ABCG2 within the epithelium, the corneal tissues were stained with a nuclear dye, DAPI, which help to discriminate basal epithelium from surface epithelium based on the density of the nuclei. As previously reported in mouse cornea, the density of the peripheral and central surface epithelial cell nuclei was lower than that of basal epithelial cells (Nagasaki and Zhao, 2003). In limbus, however, the density of surface epithelial cell was higher than that of basal epithelial cells. To further confirm the vertical location of limbal BrdU LRC, cryosections were prepared from whole-mount cornea tissues whose en face profile had been examined previously. This method made a direct comparison between an en face view and a cross-sectional view of the same cells. The results revealed that all limbal BrdU LRCs with expression of ABCG2 were located in the limbal epithelial basal layer (data not showed).

Immunofluorescence labeling of corneal tissues with MHC class II antibody showed expression of MHC class II only at the limbus (96 ± 7.8 cells/mm^2) and periphery (87 ± 2.7 cells/mm^2) of the cornea, whereas the cells in the central epithelium were all negative for MHC class II. In the limbal and peripheral corneal surface epithelia, dendrite-shaped MHC class II$^+$ cells formed a dense collar around the cornea. Simultaneous staining of BrdU LRCs containing corneal tissues with BrdU antibody revealed that these cells were all negative for BrdU labeling, whereas approximately 20% of limbal BrdU LRCs expressed MHC class II antigen (Fig. 2). This finding was confirmed by cross-sectional studies, which showed that MHC class II$^+$ BrdU-labeled cells were exclusively located in the limbal epithelial basal layer (Fig. 3). Double labeling with CD11c showed that all the MHC class II$^+$ cells in the limbal basal epithelium were positive for CD11c (Fig. 4).

Immunofluorescence labeling of corneal tissues with keratin 3 and keratin 14 revealed that keratin 14$^+$ cells were localized in the limbal and peripheral basal epithelia, while keratin 3$^+$ cells were primarily concentrated in the central area. Double staining of corneal tissues with ABCG2 and keratin 14 showed that nearly four-fifth of limbal ABCG2$^+$ cells expressed K14 (Fig. 4).

3.3. Cytospin sample analysis

As our results suggested that limbal ABCG2$^+$ cells are slow-cycling cells, we next performed double immunofluorescence staining of cytospin sample to determine the cell size and N/C ratio of these cells. Immunostaining of cytospin preparations with ABCG2 showed that of all cells isolated from normal limbal epithelium, ABCG2$^+$ cells comprised an average of $2.6 \pm 0.7\%$. Double staining with MHC class II revealed that nearly one-fifth of limbal ABCG2$^+$ cells expressed MHC class II antigen (Fig. 5). All the size of limbal ABCG2$^+$ cells was significantly smaller, whereas the N/C ratio of these cells was significantly larger than those of peripheral and central corneal epithelial cells (Table 1). However, there was no significant difference between limbal ABCG2$^+$ cells with expression of MHC class II and limbal ABCG2$^+$ cells without expression of MHC.

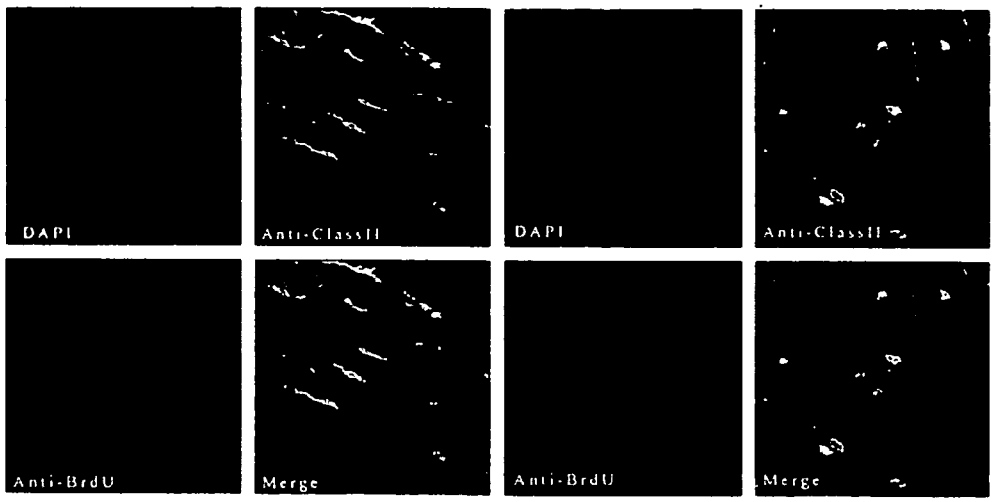

Fig. 2. Distribution of BrdU-labeled and MHC class II^+ cells in the limbal epithelium. (left) Limbal surface epithelium; (right) limbal basal epithelium. Whole-mount corneal tissues were assessed for BrdU labeling and expression of MHC class II antigen in the limbal epithelium. Confocal micrographs show significant number of dendrite-type MHC class II^+ cells in the surface epithelium of the limbus. These cells were all negative for BrdU labeling. In contrast, a number of round MHC class II^+ cells were present in the limbal basal epithelium and some of them were positive for BrdU labeling (pink). Note that the density of the limbal surface epithelial cells was higher than that of the limbal basal epithelial cells.

4. Discussion

As expected, BrdU LRCs were found to be exclusively concentrated in the limbal basal epithelium. Previous studies in mouse (Cotsarelis et al., 1989), rabbit (Wirtschafter et al., 1999), and rat (Chen et al., 2003) have demonstrated that slow-cycling cells are concentrated in the basal epithelium of the limbus but are absent from the peripheral and central corneal epithelia. Existence of slow-cycling cells in the limbal epithelium, on the one hand, coupled with the failure to routinely detect slow-cycling cells in other corneal epithelium on the other, has led to the conclusion that corneal epithelial stem cells are exclusively located in the limbus. The present study indicates that approximately $2.6 \pm 0.7\%$ of limbal epithelial cells can be identified as BrdU LRCs with expression of ABCG2. This finding is in accordance with another study reporting that corneal stem cells represent less 10% of the total limbal basal cell population (Lavker et al., 1991).

ABCG2, a member of ABC transporters, formally known as breast cancer resistance protein 1, is expressed in a wide variety of primitive stem cells (Trosko and Ruch, 1998; Zhou et al., 2001; Kim and Turnquist, 2002). Constitutive expression of ABCG2 is thought to be associated with the side population (SP) phenotype based on the ability to efflux Hoechst

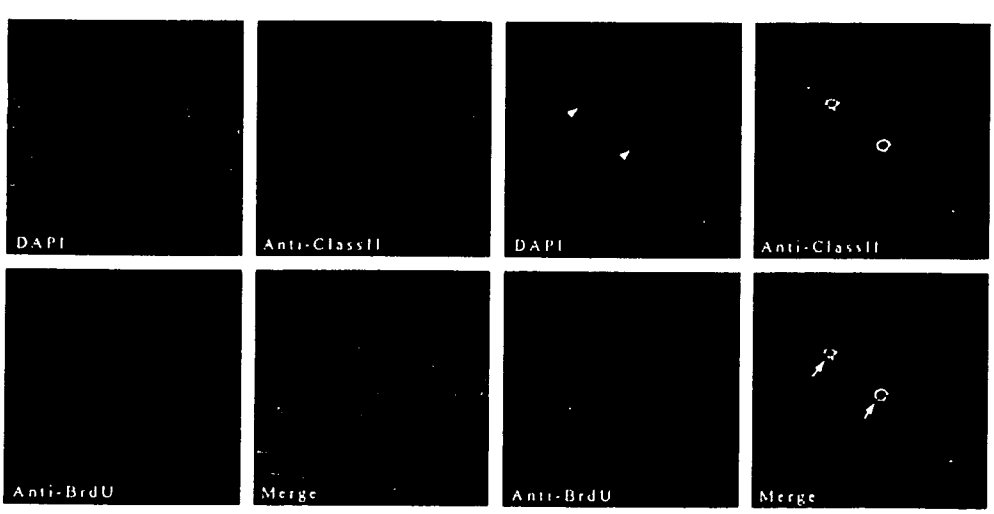

Fig. 3. Localization of MHC class II^+ BrdU LRCs in the corneal epithelium. Immunostained BrdU LRCs containing rat corneal tissues, which had been observed on whole mount, were cut into cross-sections and examined by confocal microscopy. (left) Central corneal epithelium; (right) limbal epithelium. Note that MHC class II^+ BrdU LRCs (arrow) are located in the limbal basal epithelium and the nuclei (arrowhead) of these cells are smaller compared with other limbal epithelial basal cells. In contrast, no such cells can be found in the central corneal epithelium.

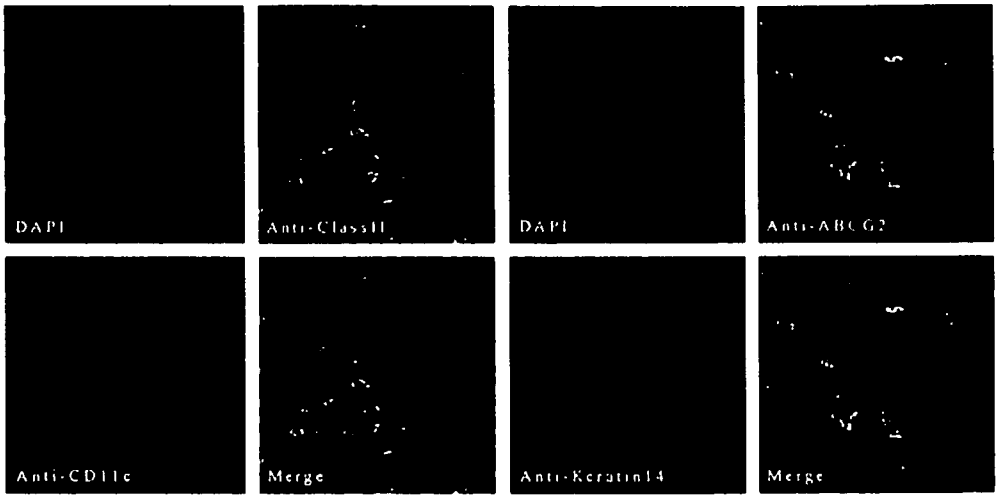

Fig. 4. Expression of MHC class II, CD11c, ABCG2 and keratin 14 in normal limbal basal epithelium. (left) All MHC class II^+ cells in limbal basal epithelium were found to be CD11c positive. (right) Double staining of normal corneal tissues with ABCG2 and K14 showed that some $ABCG2^+$ cells in limbal basal epithelium coexpressed keratin 14 (pink).

33342 dye (Zhou et al., 2001). Limbal $ABCG2^+$ cells, which represent 2.5–3% of the limbal epithelial cells, were found to exhibit greater colony-forming efficiency (CFE) on a 3T3 fibroblast feeder layer than limbal $ABCG2^-$ cells (de Paiva et al., 2005). Furthermore, semiquantitative RT-PCR revealed that the expression of ABCG2 was markedly higher in limbal than in corneal epithelia (Umemoto et al., 2005). These findings, in conjunction with immunohistochemical observation showing ABCG2 transporter is exclusively expressed by a small number of limbal basal cell, have suggested that ABCG2 is a reliable marker for identification of limbal stem cells (Schlötzer-Schrehardt and Kruse, 2005; de Paiva et al., 2005). Using an immunofluorescence double-staining technique applied to confocal microscope, we found that all $ABCG2^+$ cells were located in the limbal basal epithelium and were positive for BrdU label-retaining test. Our study provides direct evidence that in rat $ABCG2^+$ cells in the limbal basal epithelium are slow-cycling cells.

We compared the cell size and N/C ratio of limbal $ABCG2^+$ cells with those of the peripheral and central corneal epithelial cells. It has been suggested that the features that distinguish stem cells from TA cells are correlated with a fundamental difference in the cell size (Gross et al., 1987; Romano et al., 2003). In the epidermis, keratinocytes with high density are found to exhibit larger proliferative capacity (Furstenberger et al., 1986). Similarly, in skin culture the smallest keratinocyte possesses the highest clonogenicity (Barrandon and Green, 1985). In the corneal epithelia, the smallest cells with low granularity and high N/C ratios are found in the limbal basal layer (Romano et al., 2003). Our study extends these findings and confirms that limbal $ABCG2^+$ cells have smaller cell size with larger N/C ratio. Taken altogether, our data show that limbal slow-cycling cells are smaller cells with larger N/C ratio and expression of ABCG2, a limbal stem cell marker. Therefore, we believe that these cells are limbal stem cells.

In the corneal epithelium, we found that the MHC class II^+ cells were exclusively distributed in the limbal and peripheral areas. Further analysis showed that while a few dendrite-shaped MHC class II^+ cells are localized in the surface epithelium of the limbus, a number of round MHC class II^+ cells are present in the basal layer. Given that limbal slow-cycling stem cells are entirely located in the limbal epithelial basal layer, we performed double immunofluorescence staining to investigate whether the round MHC class II^+ cells present in the limbal epithelial basal layer are slow-cycling cells. Immunofluorescence staining on whole mount corneal tissues showed that some MHC class II^+ cells in limbal epithelium could be identified as BrdU LRCs, suggesting that these cells were slow-cycling cells. Cross-sectional studies further confirmed that limbal BrdU LRCs with expression of MHC class II were exclusively located in the limbal basal epithelium. Our data have demonstrated that limbal basal epithelium is indeed endowed with a small number of slow-cycling MHC class II^+ cells. We noted that all MHC class II^+ BrdU LRCs in limbal basal epithelium expressed ABCG2. Moreover, limbal $ABCG2^+$ cells with expression of MHC class II were found to be smaller cells with larger N/C ratio than peripheral and corneal epithelial cells. We also noted that there was no significant difference between limbal $ABCG2^+$ cells with expression of MHC class II and $ABCG2^+$ cells without expression of MHC class II in cellular and nuclear areas, indicating that the cell size and N/C ratio of these cells were similar.

Our results have indicated that nearly four-fifth of limbal $ABCG2^+$ cells are positive for keratin 14, a maker for undifferentiated and less proliferative corneal epithelial cells, but negative for keratin 3, a corneal epithelial differentiation marker. This finding is in agreement with the study reporting that in adult rat cornea keratin 14 positive cells are confined to the limbal and peripheral basal epithelium (Hsueh et al., 2004). In contrast, nearly one-fifth of limbal $ABCG2^+$ cells

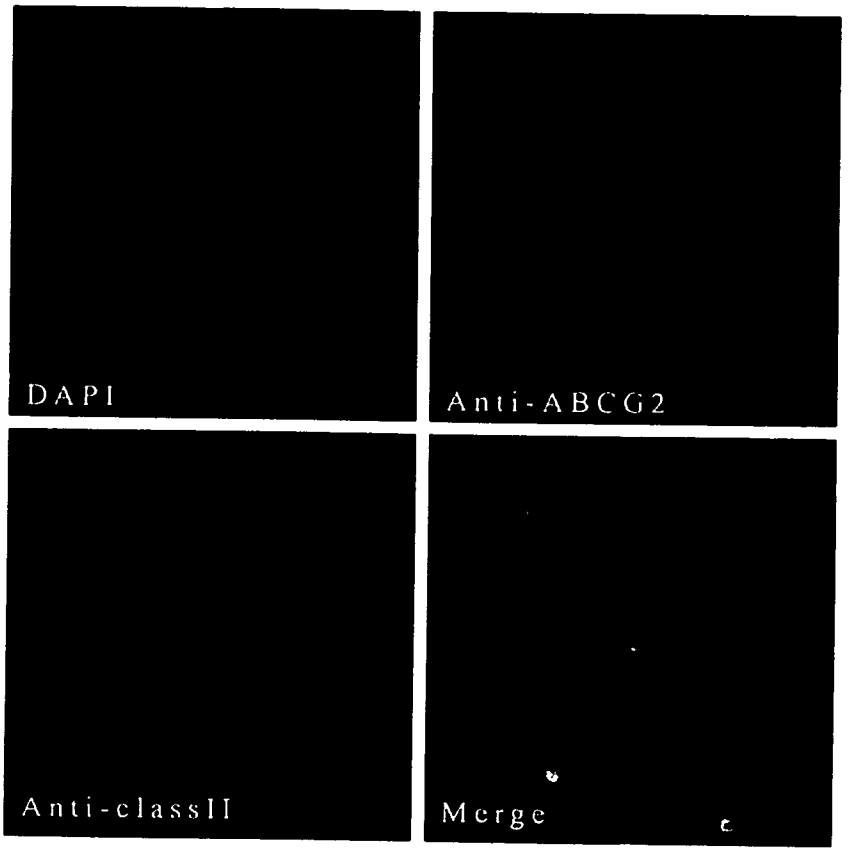

Fig. 5. ABCG2 and MHC class II staining of dissociated limbal epithelium. Representative confocal micrographs of DAPI (A, blue), ABCG2 (B, green) and MHC class II (D, red). An average of 2.6 ± 0.7% cells of limbal cells was found to be $ABCG^+$ cells. Double staining with MHC class II shows that approximately 20% of limbal $ABCG^+$ cells expressed MHC class II antigen.

are negative for keratin 14, exhibiting non-epithelium derivation. It has been demonstrated that the presence of major histocompatibility complex (MHC) class II antigens on the surface of antigen-presenting cells (APCs) has important implications for both the generation and expression of the immune response (Parham and Strominger, 1982; Mellman and Steinman, 2001). Therefore, we speculate that normal limbal basal epithelium contains at least two types of slow-cycling cells: MHC class II^- cells are the progenitor of epithelial cell, which may perform an important role in the replacement of corneal epithelium, while MHC class II^+ cells may serve as the critical sentinel cells of the immune system in the corneal epithelium. To our knowledge, we are the first group to report the existence of slow-cycling MHC class II^+ cells in the limbal basal epithelium of the uninflamed eye.

LCs have been identified as the only cells that constitutively express MHC class II molecules in normal corneal epithelium (Klareskog et al., 1979; Hamrah et al., 2002; Yamagami et al., 2005). They are the professional APCs of the corneal epithelium and serve as the critical sentinel cells

Table 1 Cell sizes measured by confocal microscopy in corneal epithelial cells

	LE $ABCG^+$ cells with expression of class II	LE $ABCG^+$ cells without expression of class II	PCEC	CCEC
Cell area (μm^2)	72.5 ± 14.3*	76.2 ± 12.1*	256.6 ± 98.5	337.5 ± 137.3
N/C ratio	0.89 ± 0.3#	0.87 ± 0.6#	0.32 ± 0.1	0.26 ± 0.1

The cell size was measured in 50 cells of each zones by confocal microscopy and data are expressed as a mean ± SD. LE, limbal epithelial, PCEC, peripheral corneal epithelial cells; CCEC, central corneal epithelial cells.
*$P < 0.005$ compared with PCEC and CCEC.
#$P < 0.001$ compared with PCEC and CCEC.
No significant difference between limbal $ABCG2^+$ with expression of MHC class II and Limbal without expression of MHC class II in cell area and N/C ratio.

of the immune system in the ocular surface (Tamaki and Katz, 1980; Gillette et al., 1982; Dana et al., 2000; Dana, 2004). Like skin LCs, corneal epithelial LCs are bone marrow-derived dendritic cells (DCs) that are capable of taking up, processing, and presenting antigen, and leading to initiation of T-lymphocyte responses (Hamrah et al., 2003). In skin, LCs are found to have a very slow turn over rate of 4 weeks and longer (Czernielewski and Demarchez, 1987; Kanitakis et al., 2004). In the present study, we found that all MHC class II^+ cells in the limbal and peripheral epithelia expressed CD11c, the marker for DC and LC. Taken these facts into account, we consider that limbal slow-cycling MHC class II^+ cells described herein may be LC precursors. Cotsarelis et al. (1989), by transmission electron microscopy, found that limbal basal epithelium is endowed with a small number of LCs. In retrospect, it is not clear whether Cotsarelis et al. were looking at the LCs that were slow-cycling cells and expressed limbal stem cell markers, e.g., ABCG2. It has been proven that inflammatory stimuli and corneal diseases result in the centripetal migration of LCs from the limbus into the central corneal epithelium (Parham and Strominger, 1982; Gillette et al., 1982; Hamrah et al., 2002). In view of the important role of LCs in immune surveillance, further studies are needed to determine the function of limbal slow-cycling MHC class II^+ LCs in corneal immune responses.

In summary, our study demonstrates existence of slow-cycling LCs in limbal basal epithelium. These findings may provide additional information for our understanding of the characteristics of limbal slow-cycling cells.

Acknowledgments

The authors thank Sanae Takaseki for her excellent technical support.

References

Arpitha, P., Prajna, N.V., Srinvasan, M., Muthukkaruppan, V., 2005. High expression of p63 combined with a large N/C ratio defines a subset of human limbal epithelial cells: implication on epithelial stem cells. Investig. Ophthalmol. Vis. Sci. 46, 3631–3636.

Barrandon, Y., Green, H., 1985. Cell size as a determinant of clone-forming ability of human keratinocytes. Proc. Natl. Acad. Sci. U.S.A. 82, 5390–5394.

Camelo, S., Shanley, A.C., Voon, A.S., McMenamin, P.G., 2004. The distribution of antigen in lymphoid tissues following its injection into the anterior chamber of the rat eye. J. Immunol. 172, 5388–5395.

Chen, W., Ishikawa, M., Yamaki, K., Sakuragi, S., 2003. Wistar rat palpebral conjunctiva contains more slow-cycling stem cells that have larger proliferative capacity. Jpn. J. Ophthalmol. 47, 119–128.

Chen, Z., de Paiva, C.S., Luo, L., Kretzer, F.L., Pflugfelder, S.C., Li, D.-Q., 2004. Characterization of putative stem cell phenotype in human limbal epithelia. Stem Cells 22, 355–366.

Cotsarelis, G., Cheng, S.Z., Dong, G., Sun, T.T., Lavker, R.M., 1989. Existence of slow-cycling limbal epithelial basal cells that can be preferentially stimulated to proliferate: implications on epithelial stem cells. Cell. 57, 201–209.

Czernielewski, J.M., Demarchez, M., 1987. Further evidence for the self-reproducing capacity of Langerhans cells in human skin. J. Investig. Dermatol. 82, 17–20.

Dana, M.R., Qian, Y., Hamrah, P., 2000. Twenty-five-year panorama of corneal immunology. Emerging concepts in the immunopathgensis of microbial keratitis, peripheral ulcerative keratitis, and corneal transplant rejection. Cornea 19, 625–643.

Dana, M.R., 2004. Corneal antigen-presenting cells: diversity, plasticity, and disguise: the cogan lecture. Investig. Ophthalmol. Vis. Sci. 45, 722–727.

Ebato, B., Friend, J., Thoft, R.A., 1988. Comparison of limbal and peripheral human corneal epithelium in tissue culture. Investig. Ophthalmol. Vis. Sci. 29, 1533–1537.

Furstenberger, G., Gross, M., Schweizer, J., et al., 1986. Isolation, characterization and in vitro cultivation of subfractions of neonatal mouse keratinocytes: effects of phorbolesters. Carcinogenesis 7, 1745–1753.

Gillette, T.E., chandler, J.W., Greiner, J.V., 1982. Langerhans cells of ocular surface. Ophthalmology 89, 700–711.

Gross, M., Furstenberger, G., Marks, F., 1987. Isolation, characterization and in vitro cultivation of subfraction from adult NMRI mouse epidermis: epidermal target cells for phorbol esters. Exp. Cell Res. 171, 460–474.

Hamrah, P., Zhang, Q., Liu, Y., Dana, R., 2002. Novel characterization of MHC class II-negative population of resident corneal Langerhans cell-type dendritic cells. Investig. Ophthalmol. Vis. Sci. 43, 639–646.

Hamrah, P., Huq, S.O., Liu, Y., Zhang, Q., Dana, M.R., 2003. Corneal immunity is mediated by heterogeneous population of antigen-presenting cells. J. Leukoc. Biol. 4, 172–176.

Hernandez Galindo, E.J., Theiss, C., Steuhl, K.P., Meller, D., 2003. Expression of Δp63 in response to phorbol ester in human limbal epithelial cells expanded on intact human amniotic membrane. Investig. Ophthalmol. Vis. Sci. 44, 2959–2965.

Higa, K., Shimmura, S., Miyashita, H., Shimazaki, J., Tsubota, K., 2005. Melanocytes in the corneal limbus interact with K19-positive basal epithelial cells. Exp. Eye Res. 81, 218–223.

Hsueh, Y.-J., Wang, D.-Y., Cheng, C.-C., Chen, J.-K., 2004. Age-related expression of p63 and other keratinocyte stem cell markers in rat cornea. J. Biomed .Sci. 11, 641–651.

Kanitakis, J., Petruzzo, P., Dubernard, J.-M., 2004. Turnover of epidermal Langerhans' cells. New Engl. J. Med. 351, 2661–2662.

Kim, M., Turnquist, H., Jackson, J., et al., 2002. The multidrug resistance transporter ABCG2(breast cancer resistance protein 1) effluxes Hoechst 33342 and is overexpressed in hematopoietic stem cells. Clin. Cancer Res. 8, 22–28.

Klareskog, L., Forsum, U., Malmnäs, T., Rask, L., Peterson, P.A., 1979. Expression of Ia antigen-like molecules on cells in the corneal epithelium. Investig. Ophthalmol. Vis. Sci. 18, 310–333.

Lavker, R.M., Dong, G., Cheng, S.Z., Kudoh, K., Cotsarelis, G., Sun, T.T., 1991. Relative proliferative rates of limbal and corneal epithelia. Implication of corneal epithelial migration, circadian rhythm, and suprabasally located DNA-synthesizing keratinocytes. Investig. Ophthalmol. Vis. Sci. 32, 1864–1875.

Lavker, R.M., Wei, Z.G., Sun, T.T., 1998. Phorbol ester preferentially stimulates mouse fornical conjunctival and limbal epithelial cells to proliferate in vivo. Investig. Ophthalmol. Vis.Sci. 39, 301–307.

Lehrer, M.S., Sun, T.T., Lavker, R.M., 1998. Strategies of epithelial repair: modulation of stem cell and transit amplifying cell proliferation. J. Cell Sci. 111, 2867–2875.

Mellman, I., Steinman, R.M., 2001. Dendritic cells: specialized and regulated antigen processing machine. Cell 106, 255–258.

Nagasaki, T., Zhao, J., 2003. Centripetal movement of corneal epithelial cells in the normal adult mouse. Investig. Ophthalmol. Vis. Sci. 44, 558–566.

Nagasaki, T., Zhao, J., 2005. Uniform distribution of epithelial stem cells in the bulbar conjunctiva. Investig. Ophthalmol. Vis. Sci. 46, 126–132.

de Paiva, C.S., Chen, Z., Corrales, R.M., Pflugfelder, S.C., Li, D.-Q., 2005. ABCG2 transporter identifies a population of clonogenic human limbal epithelial cells. Stem Cells 23, 63–73.

Parham, P., Strominger, J., 1982. Histocompatibility antigens: structure and function. Histocompatibility Antigen. Chapman and Hall, London, pp. 119–185.

Romano, A.C., Espana, E.M., Yoo, S.H., Budak, M.T., Wolosin, J.M., Tseng, S.C.G., 2003. Different cell sizes in human limbal and central corneal basal epithelia measured by confocal microscopy and flow cytometry. Investig. Ophthalmol. Vis. Sci. 44, 5125–5129.

Schlötzer-Schrehardt, U., Kruse, F.E., 2005. Identification and characterization of limbal stem cells. Exp. Eye Res. 81, 247–264.

Tamaki, K., Katz, S.I., 1980. Ontogeny of Langerhans cells. J. Investig. Dermatol. 75, 12–13.

Trosko, J.E., Ruch, R.J., 1998. Cell-cell communication in carcinogenesis. Front. Biosci. 3, D208–D236.

Umemoto, T., Yamato, M., Nishida, K., Kohno, C., et al., 2005. Rat limbal epithelial side population cells exhibit a distinct expression of stem cell markers that are lacking in side population cells from the central cornea. FEBS Lett. 579, 6569–6574.

Wirtschafter, J.D., Ketcham, J.M., Weinstock, R.J., Tabesh, T., Mcloon, L.K., 1999. Mucocutaneous junction as the major source of replacement palpebral conjunctival epithelial cells. Investig. Ophthalmol. Vis. Sci. 40, 3138–3146.

Yamagami, S., Yokoo, S., Usui, T., Yamagami, H., Amano, S., Ebihara, N., 2005. Distinct population of dendritic cells in the normal human donor corneal epithelium. Investig. Ophthalmol. Vis. Sci. 46, 4489–4494.

Zhou, S., Schuetz, J.D., Bunting, K.D., et al., 2001. The ABC transporter Bcrp1/ABCG2 is expressed in a wide variety of stem cells and is molecular determinant of side-population phenotype. Nat. Med. 7, 1028–1034.

Available online at www.sciencedirect.com
SCIENCE DIRECT
Experimental Eye Research 82 (2006) 427–440
EXPERIMENTAL EYE RESEARCH
www.elsevier.com/locate/yexer

Morphometric evaluation of changes with time in optic disc structure and thickness of retinal nerve fibre layer in chronic ocular hypertensive monkeys

Masamitsu Shimazawa[a,c], Goji Tomita[b], Takazumi Taniguchi[a], Masaaki Sasaoka[a], Hideaki Hara[a,c,*], Yoshiaki Kitazawa[d], Makoto Araie[b]

[a]*Glaucoma Group, Research and Development Center, Santen Pharmaceutical Co. Ltd, Nara, Japan*
[b]*Department of Ophthalmology, University of Tokyo School of Medicine, Tokyo, Japan*
[c]*Department of Biofunctional Molecules, Gifu Pharmaceutical University, 5-6-1 Mitahora-higashi, 502-8585 Gifu, Japan*
[d]*Department of Ophthalmology, Gifu University School of Medicine, Gifu, Japan*

Received 3 March 2005; accepted in revised form 1 August 2005
Available online 4 January 2006

Abstract

We examined the time course of changes in optic disc structure by means of a scanning laser ophthalmoscope (Heidelberg Retina Tomograph, HRT) in ocular hypertensive (experimental glaucoma) monkeys, and clarified the relationships between the histological RNFL thickness and HRT parameters. Further, the time course of changes in retinal nerve fiber layer (RNFL) thickness in individual eyes was measured using a scanning laser polarimeter with fixed corneal polarization compensator (GDx FCC). In the present study, two separate experiments were carried out. A chronic intraocular pressure (IOP) elevation was induced by laser trabeculoplasty in the left eye in 11 cynomolgus monkeys. In Experiment 1, the HRT and GDx parameters were measured 12 weeks after the laser treatment in 10 eyes in five monkeys. In Experiment 2, the time course of changes in the HRT and GDx parameters was examined before and 1, 3, 4, 5, 6, 8, 10, 12, 14, and 16 weeks after the laser treatment in 12 eyes in six monkeys. The retardation values (thickness parameters) obtained from the GDx were used to derive thickness and ratio parameters in the superior, inferior, nasal and temporal quadrants. Ratio parameters were expressed as a ratio of superior and inferior quadrant to nasal quadrant. After the last measurements, each eye was enucleated, and retinal cross sections were prepared for histological analysis.

In the left (hypertensive) eyes, IOP was persistently elevated throughout the observation periods in both Experiments 1 and 2. In the HRT measurements in Experiment 1, seven out of eight global topographic parameters (exception, disc area) were statistically different between the hypertensive and control eyes 12 weeks after the laser treatment. In Experiment 2, the HRT parameters changed in a time-dependent manner, but each of them almost plateaued at about 4 weeks after the laser treatment. Significant correlations were seen between the histological mean RNFL thickness at 1.5 disc diameters from the optic disc margin and the HRT parameters in 21 eyes from 11 monkeys in Experiments 1 and 2. Especially good correlations with histological mean RNFL thickness were seen for the rim volume and cup volume.

In Experiment 1, good correlations were found between GDx ratio parameters and histological RNFL thickness in individual right control eyes ($n=5$). In individual left experimental glaucoma eyes of Experiment 2 ($n=6$), GDx ratio parameters declined in a time-dependent manner alongside the IOP elevation.

In conclusion, alongside the IOP elevation, time-related changes in optic disc topography and RNFL thickness were demonstrated in monkey eyes using HRT and GDx. HRT (rim and cup) parameters showed good correlations with histological RNFL thickness, and significant interrelations.

Keywords: ocular hypertensive monkey; optic disc; retinal nerve fibre layer; scanning laser ophthalmoscope; scanning laser polarimeter

1. Introduction

Open-angle glaucoma (OAG) is a slowly progressive and chronic disease. To diagnose OAG, especially in its early stage, evaluation of the appearance of the optic nerve head and peripapillary retina is most important. For objective

* Corresponding author. Dr Hideaki Hara, Department of Biofunctional Molecules, Gifu Pharmaceutical University, 5-6-1 Mitahora-higashi, Gifu 502-8585, Japan.
E-mail address: hidehara@gifu-pu.ac.jp (H. Hara).

0014-4835/$ - see front matter © 2005 Elsevier Ltd. All rights reserved.
doi:10.1016/j.exer.2005.08.001

examination of these structures, the confocal scanning laser ophthalmoscope (Heidelberg retina tomograph, HRT; Heidelberg Engineering GmbH, Heidelberg, Germany) and scanning laser polarimeter (GDx; Laser Diagnostic Technologies, San Diego, CA, USA) have been developed. Analysis of HRT images allows quantitative three-dimensional optic disc topography (e.g. measurement of cup volume and rim volume), and HRT has been widely used as a research tool in topographical analysis of the optic nerve head (Malinovsky, 1996). The GDx is a scanning laser polarimeter for measuring the thickness of the peripapillary retinal nerve fibre layer (RNFL), which is directly affected by glaucoma, and this instrument can provide an objective assessment of optic nerve fibre layer thickness. The data obtained from these devices show correlations with the visual field defect in patients with OAG (Iester et al., 1997; Chen et al., 1998), and they can discriminate with certain sensitivity and specificity between eyes with glaucoma and normal eyes (Weinreb et al., 1995a; Essock et al., 2000; Wollstein et al., 2000).

Experimentally, the laser-induced ocular hypertensive monkey is a widely used animal model of glaucoma (Pederson et al., 1984; Fukuchi et al., 1992; Quigley et al., 1996). Morgan et al. (1998) reported that in a single normal monkey, the value for RNFL thickness obtained from the Mark II Nerve Fiber Analyzer (NFA, Laser Diagnostic Technologies), a prototype GDx, correlated with the histological one, while Yücel et al. (1998) noted that HRT parameters correlated with the number of optic nerve axons in 10 laser-induced ocular hypertensive monkeys. However, these studies were carried out after the glaucomatous changes had been established, and there is little information in the literature as to how the RNFL thickness alters alongside the IOP elevation. In a longitudinal study, Burgoyne et al. (1995) made a detailed examination of optic disc surface changes using digital ocular funduscopy and confocal scanning laser tomography (TopSS, Laser Diagnostic Technologies), and concluded that early changes in the optic disc surface are unlikely to be due to axon loss alone, but to damage to the load-bearing connective tissues of ONH. However, to our knowledge, no study has yet examined both the optic disc surface and RNFL thickness changes with time alongside an IOP elevation. Further, few studies have compared the in vivo HRT findings obtained just before sacrifice with findings derived from post-mortem histological examination of the retinal nerve fibre layer.

The current study had two aims. One was to examine how optic disc topography and RNFL thickness might alter alongside a chronic IOP elevation in laser-induced ocular hypertensive (experimental glaucoma) monkey eyes. The other was to compare optic disc topography (as determined using HRT) just before sacrifice with the histological findings obtained in the same eyes in a large enough number of monkey eyes for the comparison to be scientifically valid.

2. Materials and methods

2.1. Animals

A total of 11 young adult cynomolgus monkeys (*Macaca fascicularis*) weighing 4.0–6.0 kg aged 5–6 years (Keari Co. Ltd, Osaka, Japan) obtained from the same colony at the same time were used to keep the animal conditions uniformly. They were housed in an air-conditioned room at 24 ± 2 °C with $60 \pm 10\%$ humidity, and given food and water ad libitum. All investigations were in accordance with the guideline of the Statement on the Use of Animals in Ophthalmic and Vision Research, and were approved and monitored by the Institutional Animal Care and Use Committee of Santen Pharmaceutical Co. Ltd.

2.2. Induction of experimental ocular hypertension (experimental glaucoma)

An elevation of intraocular pressure (IOP) was induced in each monkey by applying the argon-laser photocoagulation burns to the trabecular meshwork of the left eye, with the right eye being used as an untreated control, as previously described (Quigley and Hohman, 1983). The laser irradiation was performed only on the left eyes, because we considered that laser irradiation on the ipsilateral eyes under the same conditions would facilitate accurate irradiation without technical dispersion. For the laser treatment, the animals were anaesthetized with an intramuscular injection of ketamine (8.75 mg kg^{-1}, Ketalar 50®; Sankyo, Tokyo, Japan) plus xylazine (0.5 mg kg^{-1}, Celactal®; Bayer, Leverkusen, Germany). Then, a single-mirror Goldmann lens filled with a hydroxyethylcellulose solution (Scopisol®15; Senjyu Pharmaceutical, Osaka, Japan) was placed on the eye to be treated. An argon blue/green laser was focused on the mid-portion of the trabecular meshwork, and a total of 150 laser-beam spots were applied around 360° (spot size, 100 μm; power, 1000 mW; exposure time, 0.2 sec) using an argon-laser photo-coagulator (Ultima 2000 SE®; Coherent, Inc., CA, USA) attached to a standard slit-lamp microscope (BQ 900; HAAG-STREIT, Köniz, Switzerland). Two weeks after the first treatment, the laser treatment was repeated so as to produce a maintained elevation in IOP. Time (in weeks) 'after the laser treatment' should be understood to date from the first of these treatments.

2.3. Experimental procedure

In this study, two separate experiments were carried out. In the first series (Experiment 1), five experimental glaucoma monkeys were used for comparison of the HRT and GDx results and fundus photographs with postmortem histological findings obtained 12 weeks after the laser treatment. IOP was measured (see below) before and at 3, 4, 6, 8, 10, and 12 weeks after the laser treatment. Baseline

IOP was taken as an average of three measurements made at 1-week intervals before the first laser treatment. All IOP measurements were carried out at the same time of day. After the last measurement, the animals were sacrificed, both eyes enucleated, and retinal cross sections prepared for histological analysis.

In the second series (Experiment 2), six monkeys were used for a study of the time course of changes in the HRT and GDx data in the experimental glaucoma eye (vs. values for the control eye) during a 16-week period after laser treatment. HRT and GDx data, and fundus photographs, were obtained before and at 1, 3, 4, 6, 8, 10, 12, 14, and 16 weeks after the laser treatment, while IOP was measured before and at 1, 2, 3, 4, 6, 8, 10, 12, 14, and 16 weeks after the laser treatment. Baseline values were taken as the average of three measurements made at 1-week intervals before the laser treatment. All IOP measurements were carried out at the same time of day. In the Experiment 2, after the last measurement, animals underwent the same procedures as in Experiment 1.

IOP was measured in both eyes of each animal using a calibrated pneumatonometer (Model 30 Classic Pneumatonometer; Medtronic Solan, FL, USA) under ketamine anaesthesia (8.75 mg kg^{-1}, i.m.), with local anaesthesia being produced using 0.4% oxibuprocaine hydrochloride (Benoxil® 0.4% solution; Santen Pharmaceutical Co. Ltd, Osaka, Japan).

Examinations (including refractometry, keratometry, fundus photography, confocal scanning laser imaging with HRT, and scanning laser polarimetry with GDx) were carried out under intramuscular ketamine (8.75 mg kg^{-1}) plus xylazine (0.5 mg kg^{-1}), and are described below in more detail.

2.4. Analysis of optic disc topography

For this analysis, the Heidelberg Retina Tomograph (HRT; Heidelberg Engineering, Heidelberg, Germany), a confocal scanning laser ophthalmoscope, was used. Just before image acquisition, the refraction and corneal curvature radius of each eye were measured using an Auto Ref/Keratometer (ARK-700A; NIDEK Co. Ltd, Aichi, Japan), and the values were entered into the Patient Data sub-menu for the examined eye to correct for magnification effects on the images. All measurements were made by the same operator (M.S.). Three images (10° field of view) of each eye were obtained by one experienced operator (M.S.), and for each pixel location, the mean of three topographic image height measurements was calculated, as previously described (Weinreb et al., 1993; Yücel et al., 1998). A good-quality mean topographic image was used; image quality of serial original images of each eye was judged qualitatively by two independent experienced observers (G.T., T.T.) and only three images judged to be of good quality were used for creating the mean image, and the mean image adopted was the one in which the optic disc morphology was clearly visible, with an overall standard deviation of less than 30 μm. The outline of the optic disc margin at the inner edge of the scleral ring was drawn by an experienced observer (G.T.) using a computer mouse system. Then, the Stereometric Measurements program (HRT software version 2.01; Heidelberg Engineering) calculated a number of predefined shape parameters.

2.5. Retinal nerve fibre layer analysis

A scanning laser polarimeter (Nerve Fiber Analyzer GDx; Laser Diagnostic Technologies, San Diego, CA, USA) was used for measuring the thickness of the retinal nerve fibre layer (RNFL). Details of its operation have been published elsewhere (Weinreb et al., 1990, 1995a,b). Briefly, the light source (a polarization-modulated laser beam; wave length, 780 nm) was directed at one point on the retina, and the reflected light (which double-passes the RNFL) was detected to obtain the retardation at that point. The laser beam was directed sequentially over each of a number of 256×256 pixels retinal locations with a field of view of approximately 15° to obtain a retardation map in which each pixel had a corresponding retardation value. All scannings were performed by the same operator (T.T.). Three retardation maps of the peripapillary retina were taken for each eye, and a baseline map was created by averaging the three retardation values corresponding to each pixel. The disc margin was drawn by an experienced operator (T.T.), who placed an ellipse to outline the inner margin of the peripapillary scleral ring. A good-quality image was used; image quality of serial original images of each eye was judged qualitatively by two independent experienced observers (G.T., M.S.) and only three images judged to be of good quality were used for creating the mean image, and the mean image adopted was the one in which the retardation map was clearly visible, with an overall standard deviation of less than 8 μm.

A measurement ellipse was then generated by the GDx instrument at 1.5–2.1 disc diameters away from and concentric with the margin of the optic disc. For analysis, we calculated thickness and ratio parameters from the pixels located within the measurement ellipse, as previously described (Xu et al., 1998). Retardation values (thickness parameters) were averaged over each 10° sector, for a total of 36 sectors. The 0° meridian is at 03:00 in the left eye and at 09:00 in the right eye. Data were downloaded into an attached personal computer and translated to a spreadsheet software program (Microsoft Excel 2000; Microsoft Corporation, Redmond, WA, USA) for analysis. The circumference was divided into four 90° quadrants: superior (50–139°), nasal (140–229°), inferior (230–319°), and temporal (320–49°), as previously described by Xu et al. (1998). In each of the nine 10° sectors in each quadrant, the superior, nasal, inferior, or temporal parameters were averaged to give the mean thickness parameter for that quadrant, and the sum of the superior and inferior thickness

parameters was termed S+I. The sum of the values obtained for the nine 10° sectors in the superior, inferior, or superior plus inferior quadrants was divided by the sum of those obtained for the nine 10° sectors in the nasal quadrant to give the ratio parameters, RaSN, RaIN, and Ra(SN+IN), respectively.

2.6. Histological examination

After the last measurements, animals were perfused via the common carotid artery with 0.5 l of 0.9% saline containing 10 U ml^{-1} heparin at room temperature, followed by 0.5 l of 4% paraformaldehyde in 0.01 mol l^{-1} phosphate-buffered saline (PBS; pH 7.4). This was done under deep sodium pentobarbital anaesthesia (30 mg kg^{-1}, i.v.; Nembutal; Abbott, North Chicago, IL, USA).

After enucleation, posterior portions of eyes were washed three times with PBS (pH 7.4), and cut to yield an area of retina with choroid and sclera (approximately 100 mm^2 and centred on the optic disc). They were fixed in 2.5% glutaraldehyde and 2% paraformaldehyde in PBS (pH 7.4) for at least 48 h at 4 °C, then embedded in paraffin. When posterior portions of the eyes were embedded in paraffin, they were aligned to correspond to the GDx image with blood vessels as an index in each eye. As shown in Fig. 1, retinal cross sections containing the optic disc were cut vertically at 100 μm intervals (each section, 3 μm thickness), then stained with haematoxylin and eosin. In five right control eyes in five monkeys in Experiment 1, the RNFL thickness from histological specimens was measured at seven locations between 1.5 and 2.1 disc diameters in

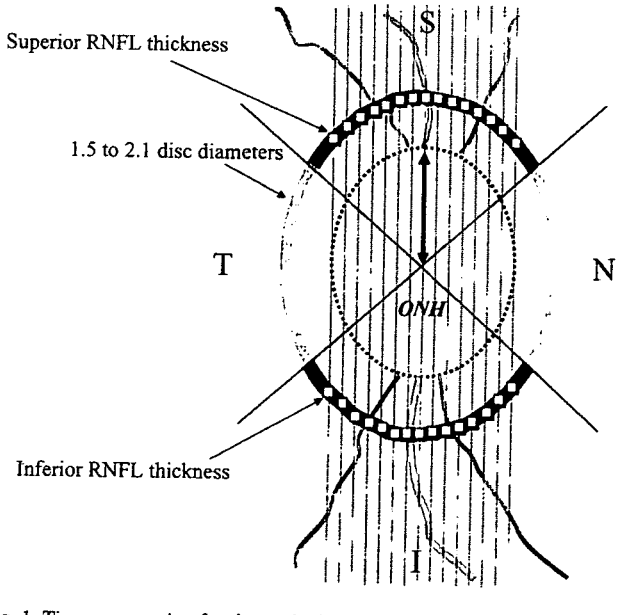

Fig. 1. Tissue processing for the analysis of histological mean retinal nerve fibre layer (RNFL) thickness. Vertical cross sections were prepared at 0.1 mm intervals, and their thickness at 1.5–2.1 disc diameters away from the optic nerve head (ONH) was measured in the superior (S) and inferior (I) quadrants. Mean thickness parameter was calculated for each of these quadrant. T, temporal quadrant; N, nasal quadrant.

0.1 disc-diameter increments away from the outer edge of the optic disc rim, and the mean RNFL thickness in superior and inferior quadrants was calculated to allow comparison with the values for GDx parameters obtained in each disc diameter in the same eye just before sacrifice.

The RNFL thickness in histological specimens was measured only at 1.5 disc diameters away from the edge of the optic disc in five left experimental glaucoma eyes (excluding one with corneal opacity) and six right control eyes of six monkeys in Experiment 2.

2.7. Statistical analysis

Data are expressed as mean±SE. In Experiment 1, statistical analysis of the experimental glaucoma versus control eyes was performed using t-test with or without the modification of an Aspin-Welch as appropriate. A repeated-measures analysis with a general linear mixed-model for estimating an interaction effect between group (left experimental glaucoma and right control eyes) and time was used to examine the time course of changes in IOP in both experiments and in the HRT parameters in Experiment 2 using the Proc Mixed of the SAS package (SAS ver. 8.2, SAS Institute, Inc., Cary, USA). If the interaction effect was significant ($p<0.05$), the t-test with Bonferroni's correction was carried out at each time-point for comparison between the experimental glaucoma and control eyes, and a paired Dunnett's multiple-comparison test was performed for comparison between the pre-laser treatment and post-laser treatment values. Pearson correlation coefficient was calculated between the mean RNFL thickness in histological specimens and the HRT parameters or between GDx and HRT parameters in a total of 21 eyes of 11 monkeys, and between the mean RNFL thickness in histological specimens and the GDx parameters in each of five right control eyes in Experiment 1, after confirming no significant deviation from normal distribution on scatter plotting of data. Results were considered to show significant difference if $p<0.05$.

3. Results

3.1. Intraocular pressure (IOP)

In Experiment 1, the baseline IOP (before laser treatment) was 19.1±0.7 mmHg ($n=5$) in the right eye and 18.7±1.0 mmHg ($n=5$) in the left eye. In the experimental glaucoma eyes, IOP was persistently elevated throughout the 12 weeks after laser treatment, being statistically significant after 3, 4, 6, 8, 10, and 12 weeks versus the IOP of the right control eye or the pre-laser treatment value (Fig. 2). There was a significant interaction effect ($p<0.001$) between the group treatments and the time for IOP. In contrast, there were no significant changes

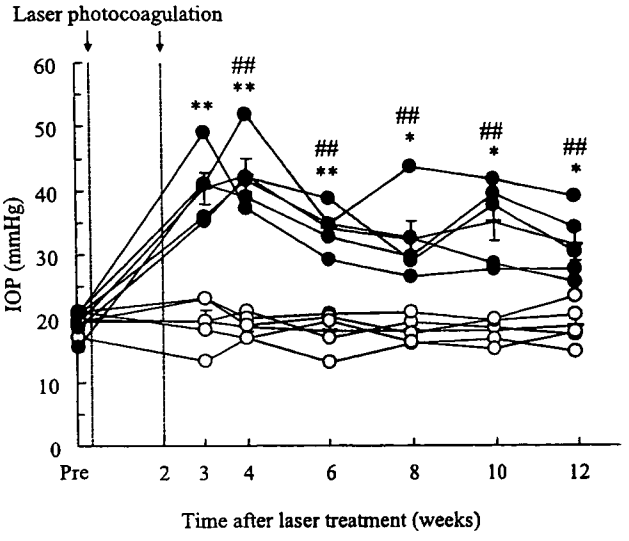

Fig. 2. Time change in IOP in each right control eye (open circle) and left experimental glaucoma eye (closed circle) in Experiment 1. There was a significant interaction effect ($p<0.001$) between the group (treatment) and time on IOP using a mixed model followed both by a t-test with Bonferroni's correction (*$p<0.05$, **$p<0.01$ vs. right control eye) and by a paired Dunnett's multiple-comparison test (## $p<0.01$ vs. pre-laser treatment values). $n=5$. Thick horizontal lines and vertical bars indicate mean ± SE.

($p>0.05$) in the control eyes versus the pre-laser treatment value.

In Experiment 2, the baseline IOP before laser treatment was 18.4 ± 1.1 mmHg ($n=6$) in the right eye and 18.3 ± 1.1 mmHg ($n=6$) in the left eye. For the experimental glaucoma eyes, IOP was persistently elevated for 16 weeks, being statistically significant after 3, 4, 5, 6, 8, 10, 12, 14, and 16 weeks versus the IOP in the control eye or the pre-laser treatment value (Fig. 3).

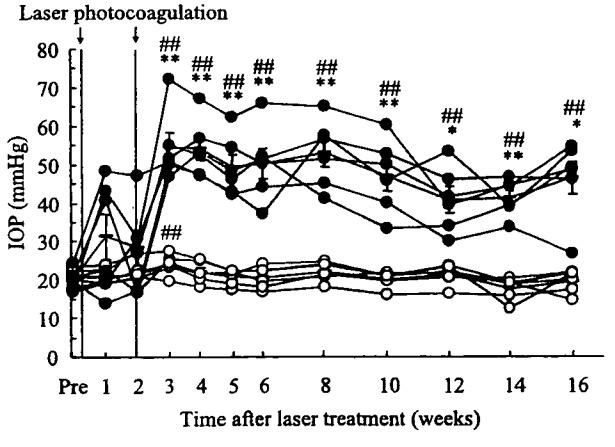

Fig. 3. Time change in IOP in each right control eye (open circle) and left experimental glaucoma eye (closed circle) in Experiment 2. There was a significant interaction effect ($p<0.001$) between group (treatment) and time on IOP using a mixed model followed both by a t-test with Bonferroni's correction (*$p<0.05$, **$p<0.01$ vs. right control eye) and by a paired Dunnett's multiple-comparison test (## $p<0.01$ vs. pre-laser treatment values). $n=6$. Thick horizontal lines and vertical bars indicate mean ± SE.

There was a significant interaction effect ($p<0.001$) between the group treatments and the time for IOP. In contrast, there were no significant changes in the control eyes, except for the IOP increase ($p=0.002$) after 3 weeks versus the pre-laser treatment value.

3.2. Fundus photography

Ocular fundus photographs taken of both the eyes of a single monkey (animal No. 1) 12 weeks after laser treatment are shown in Fig. 4. In comparison with the control eye (Fig. 4a), the experimental glaucoma eye (Fig. 4B) exhibited deepened and enlarged optic disc cupping, nerve fibre layer thinning, and peripapillary choroidal atrophy. These changes were seen in all laser-induced experimental glaucoma eyes of 11 monkeys.

3.3. Optic disc topography

Topographic images of the optic nerve head obtained using HRT for both the eyes of a single monkey (animal No. 1) 12 weeks after laser treatment in Experiment 1 are shown in Fig. 5. Mean values for the optic disc topographic parameters in the control and experimental glaucoma eyes of five monkeys are shown in Table 1. Seven of the eight global topographic parameters showed statistically significant differences between the two eyes, the exception being the disc area. Differences in the rim area and height variation contour were still significant ($p<0.0063$) after correcting the p-value by the number of comparisons, which totalled eight parameters.

Over the time course of changes in Experiment 2, baseline values were taken as the average of three measurements made at 1-week intervals before the laser treatment, and confirmed that there was no significant right–left difference in any of the HRT parameters examined. From the variation in the baseline data ($n=6$), changes greater than 4.6% for the rim area, 9.7% for the height variation contour, 10.6% for the rim volume, 10.5% for the mean RNFL thickness, 36.6% for the cup volume, 18.4% for the cup shape measure and 7.3% for the mean cup depth (% change vs. baseline value) would be detected with $n=6$ with a significance level (α) of 0.05 using the Dunnett's critical value for 10 groups of 2.6862 and statistical power ($1-\alpha$) of 0.8. The time course of the changes for the average of the HRT parameters in Experiment 2 is shown in Fig. 6. There were significant interaction effects between group treatments and time for all parameters except the disc area ($p=0.997$). For the experimental glaucoma eyes, all the HRT parameters except the disc area changed in a time-dependent manner, but almost plateaued 4 weeks after the laser treatment. In contrast, there were no significant changes ($p>0.05$) in the control eyes vs. the pre-laser treatment value. To determine the rate of change in individual eyes, the mean ± 3SD values including 99.6% distribution for individual